MASTER OF SCIENCE

Towards covalent inhibition of phosphoglucomutase in Aspergillus fumigatus

Kowalski, Bartosz

Award date:
2023

Towards covalent inhibition of phosphoglucomutase in *Aspergillus fumigatus*

Bartosz Leszek Kowalski

Supervisor – Professor Daan van Aalten

MSc Life Sciences by Research

University of Dundee,

School of Life Sciences

May 2023

Contents

List of Figures

List of Tables

Acknowledgements

The last two years have taught me how to independently manage a research project, an experience that will be invaluable in the near future. I would like to thank my supervisor, Prof. Daan van Aalten for hosting and fostering this project. I would also like to express gratitude to Dr David Murray for proofreading my work and for the occasional good word.

I thank my colleagues and day-to-day mentors, Dr Kaizhou Yan and Dr Matthew Stanley, for long philosophical debates, disagreements and advice on experiments.

Last but not least, I would like to thank the School of Life Sciences at Dundee University for providing the funding for this work.

Declaration

Declaration: I hereby declare that the candidate is the author of the thesis and all references cited have been consulted by the candidate. Unless otherwise indicated, the work in the thesis has been done by the candidate. Finally, the thesis has not previously been submitted for any degree

Prof. Daan van Aalten

Bartosz Kowalski

List of publications

Yan, K.; Stanley, M.; **Kowalski, B**.; Raimi, O. G.; Ferenbach, A. T.; Wei, P.; Fang, W.; van Aalten, D. M. F. Genetic Validation of *Aspergillus Fumigatus* Phosphoglucomutase as a Viable Therapeutic Target in Invasive Aspergillosis. J. Biol. Chem. 2022, 298 (6), 102003. https://doi.org/10.1016/j.jbc.2022.102003

Zhou, Y.; Yan, K.; Qin, Q.; Raimi, O. G.; Du, C.; Wang, B.; Ahamefule, C. S.; **Kowalski, B**.; Jin, C.; van Aalten, D. M. F.; Fang, W. Phosphoglucose Isomerase Is Important for *Aspergillus Fumigatus* Cell Wall Biogenesis. MBio 2022, 13 (4). https://doi.org/10.1128/mbio.01426-22.

Abbreviations

AGM	N-acetylphosphoglucosamine mutase
CPM	7-Diethylamino-3-(4'-Maleimidylphenyl)-4-Methylcoumarin
FBDD	Fragment-based Drug Discovery
G-1,6-bP	Glucose-1,6-bis-Phosphate
G1P	Glucose-1-Phosphate
G6P	Glucose-6-Phosphate
G6PDH	Glucose-6-Phosphate Dehydrogenase
GlcN	Glucosamine
GNA	Glucosamine-phosphate N-acetyltransferase
HXK	Hexokinase
IC_{50}	Half maximal inhibitory concentration
ISFP	Isothiazolone Fragment of PGM
k_{cat}	Turnover rate
K_i	Inhibitory constant
k_{inact}	Maximal rate of inactivation
K_m	Michaelis-Menten constant
LC-MS	Liquid Chromatography and Mass Spectrometry tandem
*Lm*G6PDH	Leuconostoc mesenteroides Glucose-6-Phosphate Dehydrogenase
Man	Mannose
NADP+	Nicotinamide adenine dinucleotide phosphate
NADPH	Reduced NADP+
NPM	N-phenyl Maleimide
PGI	Phosphoglucoisomerase
PGM	Phosphoglucomutase
TPH	Trehalose Hydrolase
TPS1	Trehalose Synthase

TPS2	Trehalose Phosphatase
Tre	Trehalose
UAP1	UDP-N-acetylglucosamine pyrophosphorylase
V_{max}	Enzyme maximal velocity

Abstract

Aspergillus fumigatus, an opportunistic fungal pathogen, is a causative agent of life-threatening invasive aspergillosis. Phosphoglucomutase 1 (PGM) is a critical enzyme interconverting glucose-1-phosphate and glucose-6-phosphate, participating in both biogenesis of the cell wall and trehalose metabolism. Here, it is demonstrated that recombinantly expressed *Af*PGM can be covalently inhibited via a cysteine residue (C353) not conserved in the human orthologue. Two mechanistically dissimilar probes were utilised to interrogate the enzyme and its mutein, showing that inhibition is elicited exclusively via cysteine C353. Preliminary data also indicated that labelling cysteine C353 with used inhibitors does not destabilise the enzyme but precludes the motion of key domains resulting in ineffective phosphoryl transfer.

Graphical abstract

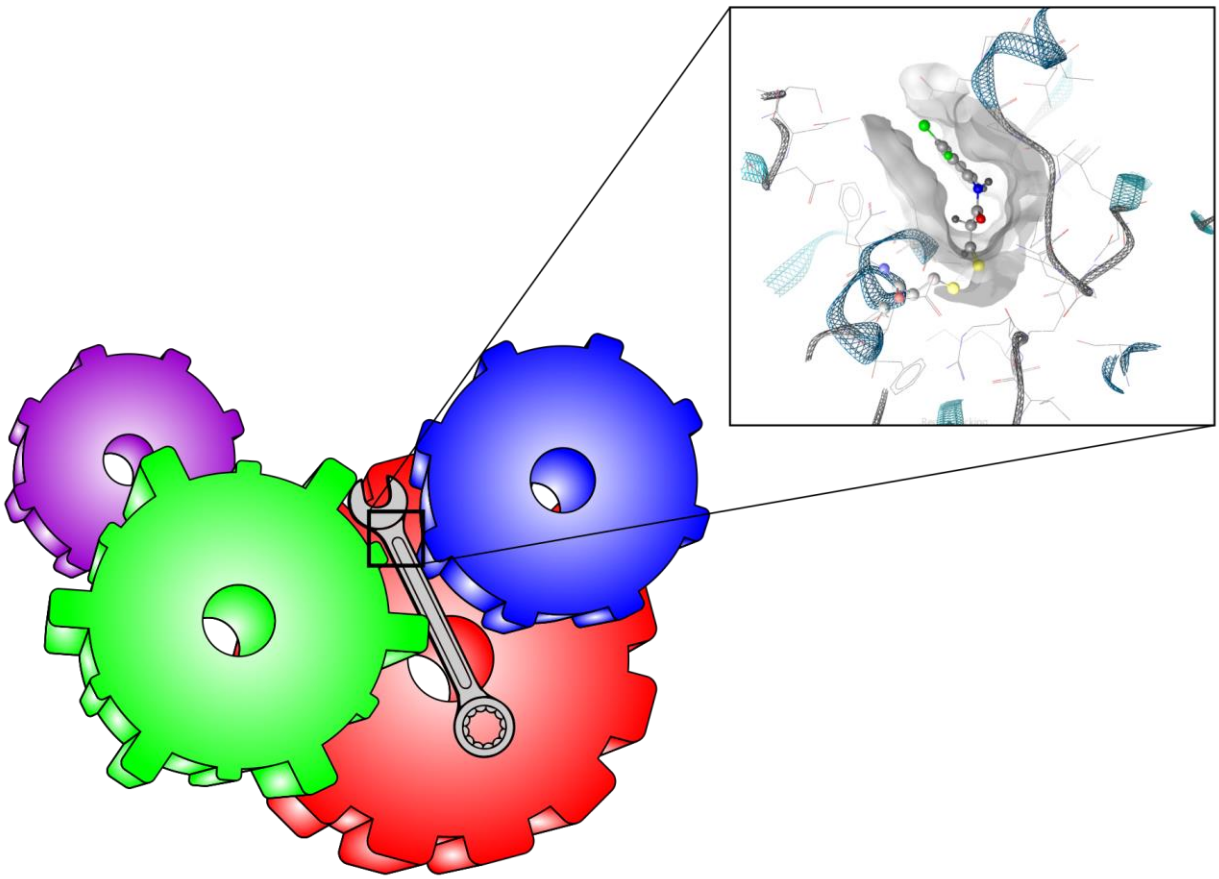

Introduction

In contrast to the environmental omnipresence of fungi, their infections are neither common nor severe in healthy populations[1]. However, immunocompromised individuals[2], those with chronic illnesses[3] and COVID-19 convalescents[4] are prone to fungi-related diseases. The most common opportunistic pathogenic fungi in neutropenic populations are *Aspergillus* and *Candida* spp.[5] Candidiasis may range from superficial non-life threatening infections to a systemic disease, with a high mortality rate of up to 71%[6]. Aspergillosis is primarily associated with severe respiratory conditions. *Aspergillus fumigatus* infections include allergic bronchopulmonary aspergillosis (ABPA)[7] and chronic pulmonary aspergillosis (CPA)[3]. Invasive aspergillosis (IA) is a condition when the infection disseminates from the lungs to other organs. With current treatment, and depending on the detection stage, the prognosis of IA is poor, giving between 15-5% survivability chance[8].

Current monotherapies (a single drug class treatment) for life-threatening mycotic infections are at least twenty years old. The traditional treatment of *Aspergillus* and *Candida spp.* infections utilise a limited repertoire of approved drugs, encompassing polyenes (approved in 1953)[9], azoles (approved in 1981)[10] and echinocandins (approved in 2001)[11].

Polyenes are natural products derived from *Streptomyces spp.*[12]. Amphotericin B (AMB) is still a gold standard in treating systemic fungal infections[13]. AMB binds with the lipid bilayer and forms a complex with ergosterol, a unique and the most abundant sterol in fungal cell membranes[14], producing pores and promoting leakage of the cellular content[15]. Although AMB is considered the most potent antifungal agent, it is not used as the first line of treatment. AMB's high lipophilicity makes its use a high risk due to the presence of cholesterol in multiple organs. Thus, it is applied only in severe and life-threatening conditions[16].

Azoles introduced a new era in managing and treating fungal infections[17]. Triazoles are the most widely used drugs as the first line of treatment against invasive aspergillosis and secondary therapy for systemic candidiasis[18,19]. Azoles target the production of ergosterol by interfering with cytochrome P450, disrupting membrane fluidity, and altering cellular growth and proliferation[20]. The last three decades have seen a significant improvement in azole design[21]. Currently, marketed drugs are relatively safe[22] however, their effectiveness has diminished. The widespread use of azoles in agriculture has led to an emergence of azole resistance in *Aspergillus* strains as collateral, rendering the therapy increasingly obsolete[16,23,24]. Over the last five years, the rate of *A. fumigatus* isolates, derived from cystic fibrosis patients, resistant to at least one azole has reached 15%[25].

Contrastingly to azoles and polyenes, echinocandins target the biosynthesis of the fungal cell wall. This class is the newest addition to antimycotics, comprising three FDA-approved drugs: caspofungin, micafungin and anidulafungin[11]. Echinocandins non-competitively inhibit the β-1,3-glucan synthase complex, disrupting cell wall dynamics and leading to osmotic instability and fungus death[15]. However, while echinocandins are successfully applied in clearing *Candida spp*. infections, their effectiveness against *Aspergillus spp*. is limited to eliciting fungistatic effects[26].

Antifungal pipeline, an unmet need.

Throughout the last two decades, no new classes of antifungals for life-threatening aspergillosis and candidiasis have been discovered[27]. In 2021, FDA approved Ibrexafungerp, the first-in-class triterpenoid, for treating non-life-threatening recurrent vulvovaginal candidiasis[28]. Ibrexafungerp inhibits the β-1,3-glucan synthase complex, but its structural dissimilarity to echinocandins allows the treatment of echinocandins-resistant *Candida spp.*[29]. Ongoing clinical trials are concentrated on applying Ibrexafungerp for invasive candidiasis therapy[30].

The approval of Ibrexafungerp is a significant step in filling the gap in antifungal development, especially against *Candida spp*. However, *Aspergillus fumigatus* and aspergillosis remain a major health problem[31]. Throughout the last twenty years the frequency of *Aspergillus fumigatus* infections increased four-fold in leukaemia patients[32]. Statistics indicate that annually 650,000 people suffer invasive aspergillosis, and with current treatment, only 15% will survive[33]. Aspergillosis also increasingly burdens non-neutropenic populations[34]. It is estimated that globally 12 million patients a year with underlying co-morbidities will be affected by *Aspergillus fumigatus*, severely decreasing their life quality and expectancy[35,36]. The need for novel agents targeting *A. fumigatus* infection is urgent, and two promising molecules, Olorofim and Fosmanogepix, are currently in clinical trials[37].

Olorofim represents a new class of antifungals: orotomides[38]. It selectively targets pyrimidine biosynthesis, reversibly engaging fungal dihydroorotate dehydrogenase[37]. Olorofim has limited activity against *Candida spp.*[39]. However, it elicits fungistatic effects towards *Aspergillus spp*. including *Aspergillus fumigatus*, with potential fungicidal effects in prolonged use[38].

Fosmanogepix, a prodrug of manogepix, is the first-in-class molecule selectively interfering with Gwt1 responsible for the co-localisation of glycosylphosphatidylinositol-anchored mannoproteins in yeast[40]. Remarkably, manogepix appears to have a broad antifungal spectrum, effective against yeasts and moulds, including azole-resistant *Aspergillus fumigatus*[41].

Several molecules are also at the advanced pre-clinical stage, showing promising results[42]. Geldanamycin targeting activation of Heat shock protein 90 (HSP90), originally intended as an antibiotic, found its application in cancer treatment[43,44]. However, combining geldanamycin with caspofungin elicits fungicidal effects in azole and echinocandins-resistant *A. fumigatus strains*[45]. Another promising strategy involves inhibiting fungal growth by arresting histones' activation via histone deacetylase inhibition by repurposing anti-cancer drugs[46].

Although Olorifim, Fosmanogepix and others are currently in clinical trials, their success is uncertain. It is estimated that 90% of drug candidates will fail in clinical trials[47]. Therefore it is essential to continue the search for exploitable targets allowing the development of new antibiotics against *Aspergillus fumigatus*. Our group has contributed to efforts aiming for novel antimycotic agents for fifteen years[48]. We focus on the fungal cell wall biogenesis providing genetic and structural validation of essential enzymes (**Figure 1**, highlighted in green) participating in this unique process.

Cell wall a unique organelle of *Aspergillus fumigatus*.

The architecture of the cell wall is unique to fungi[49,50]. It is often described as ordered but subjected to constant remodelling depending on the environmental circumstances[51]. The fungal cell wall is primarily composed of polymeric carbohydrates, mostly glucans, chitin, galactomannan and glycosaminoglycan[52].

In *Aspergillus fumigatus*, the most predominant form of glucan β-1,3-glucan, assembled by the glucan synthase complex, using UDP-glucose as a building block[53]. The central role of β-1,3-glucans is to protect cells from a hostile environment and to anchor other cell wall components[54]. The absence of β-1,3 glucan synthase in humans has made it an attractive target for antimycotic development, resulting in the discovery of echinocandins[15,55]and the most recent, Ibrexafungerp, a novel triterpenoid[28]. Echinocandins and Ibrexafungerp non-competitively inhibit a glucan synthase complex (FKs1 subunit), disrupting the cell wall dynamics. Echinocandins are widely used in clearing *Candids spp*. infections[56]. However, they are only fungistatic against *Aspergillus fumigatus* due to compensatory mechanisms triggering overexpression of chitin synthases[57]. Although Ibrexafungerp is structurally dissimilar to echinocandins and occupies a different binding site at the glucan synthase, there is not enough evidence to support its use as a monotherapy in aspergillosis[58].

Chitin is another vital component of the fungal cell wall absent in humans. It is assembled from a β-1,4 linked homopolymer of N-acetylglucosamine by a large family of enzymes called chitin

synthases[59]. The chitin synthases (CHS) are encoded by multiple genes that provide them with functional redundancy, linked to difficulties developing inhibitors[60]. Nikkomycins are nucleoside peptides and are currently the only known modulators of CHS. They compete with UDP-*N*-acetylglucosamine in the chitin synthase active site[61]. Nikkomycins have a minor potential as antifungals, and their therapeutic usefulness against *A. fumigatus* and *C. albicans* comes only in combined therapy with echinocandins[51].

In *Aspergillus fumigatus*, mannans take the form of galactomannan (GM), assembled from α-1,2 and α-1,6-mannan linked with side chains of β-1,5-galactofuran[62]. Although the detailed mechanism of galactomannan biosynthesis is still unknown, the polymer is not synthesised by transmembrane glycosyl-transferases like glucan and chitin but assembled in Golgi[63]. The structural role of galactomannan is still poorly understood[64], however, it plays a significant part in the modulation of the host immune response[65]. Contrastingly to other cell wall components, GM is not only present within the cell wall but also actively secreted. Moreover, galactomannan is an important clinical marker, indicating systemic aspergillosis[66]. Similarly to chitin synthases, mannosyltransferases are encoded by multiple genes, providing them with functional redundancy[63]. Although there are currently no approved drugs targeting mannosyltransferases, manogepix and its prodrug fosmanogepix interfere with trafficking and anchoring mannosylated proteins in yeast[40]. Initially, manogepix intended for treating *Candida spp*. infections appeared to have a broad action spectrum, including rare moulds and *Aspergillus fumigatus*[41].

Taking a step back from glycosyltransferases

Glycosyltransferases participating in the biogenesis of the fungal cell wall are not conserved in humans. Thus they constitute the most attractive strategy for developing selective antifungals. However, their functional redundancy, the existence of the compensatory pathways and a limited scope of putative targets make them challenging to exploit[59,60,67].

Glycosyl transferases are carbohydrate-nucleotide processing enzymes. Disrupting the flux of specific sugar nucleotides to these enzymes has been demonstrated to impact the cell wall composition, thus having a detrimental effect on fungi[68–70]. Focusing on the biosynthesis of the sugar nucleotides also increases the number of putative targets (**Figure 1**). However, increasing the scope of targets comes at a price. The same enzymes participating in the biosynthesis of sugar nucleotides are conserved in humans, and attempts for non-selective inhibition may have severe consequences, including

congenital disorders of glycosylation[71]. Additionally, not all enzymes participating in the biosynthesis of the fungal cell wall must be essential for different species. Some may display functional redundancy, or their inhibition/ deletion may trigger unknown compensatory pathways, preserving fungal viability[72]. Genetic validation, an assessment of gene essentiality for fungal viability or virulence, is a cornerstone of this approach[73].

The second pillar of targeting sugar nucleotide biosynthetic pathways is the development of selective chemical probes that would engage the proteins of interest[69]. As mentioned, enzymes participating in the biosynthesis of carbohydrate nucleotides are conserved in humans. However, the degree of sequence identity between fungal and human orthologues varies, allowing for mapping non-conserved pockets or residues exploitable for developing selective inhibitors[70].

Fragment-based drug discovery (FBBD) is a well-established process for discovering novel chemical entities[74]. Fragments were historically described as small molecules below 300 Da, having three or fewer hydrogen bond donors and acceptors and hydrophobicity to hydrophilicity ratio (cLogP) lower than three[75]. The currently adopted definition of fragments is far broader, and numerous commercial libraries offer various approaches, including general and targeted libraries designed for specific techniques[76,77]. Compared to drug-like molecules or natural products, fragment screens offer much more extensive coverage of chemical space with fewer molecules, better binding efficiency and lower cost[78,79]. Although natural products and drug-like molecules are still used in drug discovery campaigns, fragments are more efficient mapping shallow and allosteric pockets[80]. The major drawback of pursuing FBBD is the need to use robust and sensitive techniques. Fragments tend to bind their targets weakly, eliciting only minor changes and requiring orthogonal techniques[81].

Biolayer interferometry (BLI) originated as a technique for assessing the kinetics of protein-protein interactions[82]. It was later repurposed for use in kinetics between small molecules and proteins[83]. Our group chose a combination of Biolayer Interferometry fragments screens with crystallographic fragments screens[84] to map non-conserved pockets in fungal enzymes.

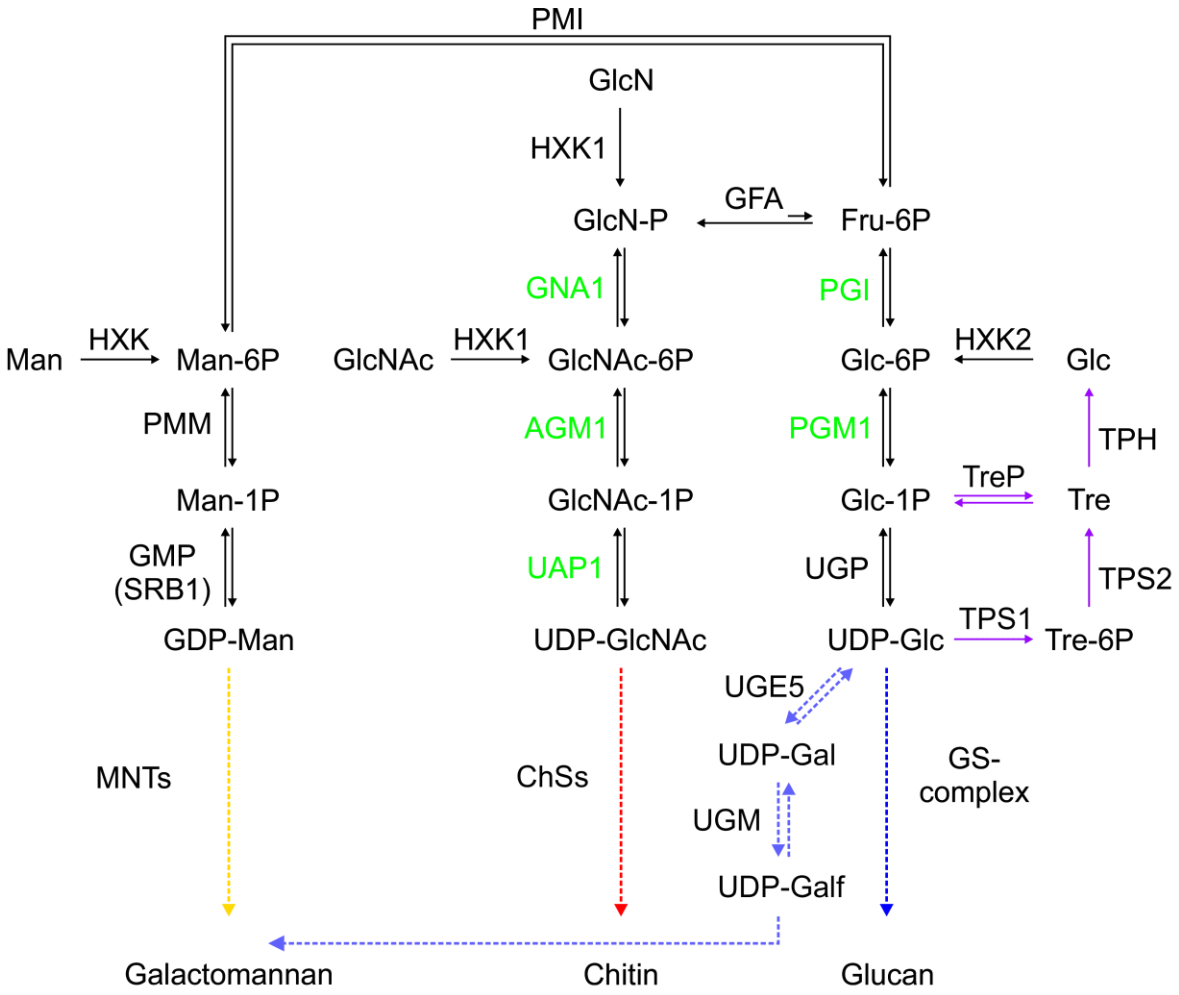

Figure 1 Biosynthesis of the fungal cell wall and trehalose from sugar nucleotides in *A.fumigatus.* The cell wall components are synthesised from three carbohydrate nucleotide precursors: GDP-Man, UDP-GlcNac and UDP-Glc. The violet pathway highlights trehalose (Tre) biogenesis. Trehalose can be synthesised from UDP-Glc or by trehalose phosphate synthase 1 or Glc-1P by trehalose phosphorylase. Enzymes highlighted in green have been genetically and structurally validated by our group. Enzymes (PMI- phosphomannoisomerase; HXK- hexokinase; GMP- mannose-1-phosphate guanyltransferase; MNTs- mannosyl transferases; GNA1- glucosamine-6-phosphate acetyltransferase; AGM1- phosphoacetylglucosamine mutase; UAP1- UDP-*N*-acetylhexosamine pyrophosphorylase; ChSs- chitin synthases; PGI- Phosphoglucoisomerase; PGM– phosphogucomutase; UGP- UTP-glucose-1-phosphate uridylyltransferase; UGE5- UDP-glucose-4-epimerase 5; UGM- UDP-galactopyranose mutase; TPS1- trehalose-6-phosphate synthase; TPS2- trehalose-6-phosphate phosphatase; TPH- trehalose hydrolase) carbohydrates and sugar nucleotides (Man- mannose; Man-6P- mannose 6-phosphate; GDP-man- GDP-mannose; GlcN- glucosamine; GlcNAc-6P- N-acetyl glucosamine-6-phosphate; GlcNAc-1P- N-acetyl glucosamine-1-phosphate; UDP-GlcNAc- UDP-*N*-acetyl glucosamine; Fru-6P- fructose-6-phosphate; Glc-6P- glucose-6-phosphate; Glc-1P- glucose-1-phosphate; UDP-Glc- UDP-Glucose; UDP-Gal- UDP-galactose; UDP-Galf- UDP-galactofuranose; Tre-6P- trehalose-6-phosphate, Tre- trehalose, Glc- glucose).

Aspergillus fumigatus Phosphoglucomutase 1- essential and druggable target

Throughout the last decade, our group provided several genetically and structurally validated enzymes crucial for the biogenesis of the fungal cell wall, including *Af*GNA1[48,69], *Af*UPA1[73], *Af*AGM1[68] and the two most recent *Af*PGM[70] and *Af*PGI[85] (**Figure 1**, highlighted in green). The high throughput fragment screens did not yield many promising hits, although in the case of *Af*GNA1, a fragment hit mapped a non-conserved pocket at the interface of the *Af*GNA1 dimer[69]. However, further molecule development did not result in the development of a potent *Af*GNA1 inhibitor. *Af*PGM, phosphoglucomutase 1, stands out as a promising target with a potentially unique mechanism of inhibition.

*Af*PGM belongs to the superfamily of α-phosphohexomutases (PHM) and a subgroup of phosphoglucomutases, facilitating interconversion between glucose-1-phosphate (G1P) and glucose-6-phosphate (G6P) via a glucose-1,6-bisphosphate (G1,6bP) intermediate[86]. The interconversion of phosphorylated carbohydrates occurs via a flip mechanism, conserved among PHMs[87,88]. The phosphoryl transfer can be divided into six steps, and the pre-requisite for the G1P and G6P interconversion is phosphorylation of the catalytic serine, either by kinase or glucose 1,6-bisphosphate. In step 1, G6P binds to the PGM in an open conformation, causing domain IV to "close" over the active cleft. Subsequently, the anomeric oxygen performs a nucleophilic attack on the phosphorus atom of the phosphorylated serine (**Figure 2**) in *Af*PGM S114 and *Ca*PGM and *Hs*PGM S117, respectively transferring the phosphate onto the sugar. In step 3, the glucose-1,6-bisphosphate undergoes a flip along the z-axis, exposing the phosphorylated oxygen in position 6 to the catalytic serine. In step 5, a hydroxyl group of the catalytic serine residue performs a nucleophilic attack on the phosphorus in position 6 of the glucose-1,6-bisphosphate, transferring the phosphate back onto the catalytic serine residue. In step 6, domain IV "opens" the active site releasing glucose-1-phosphate[89].

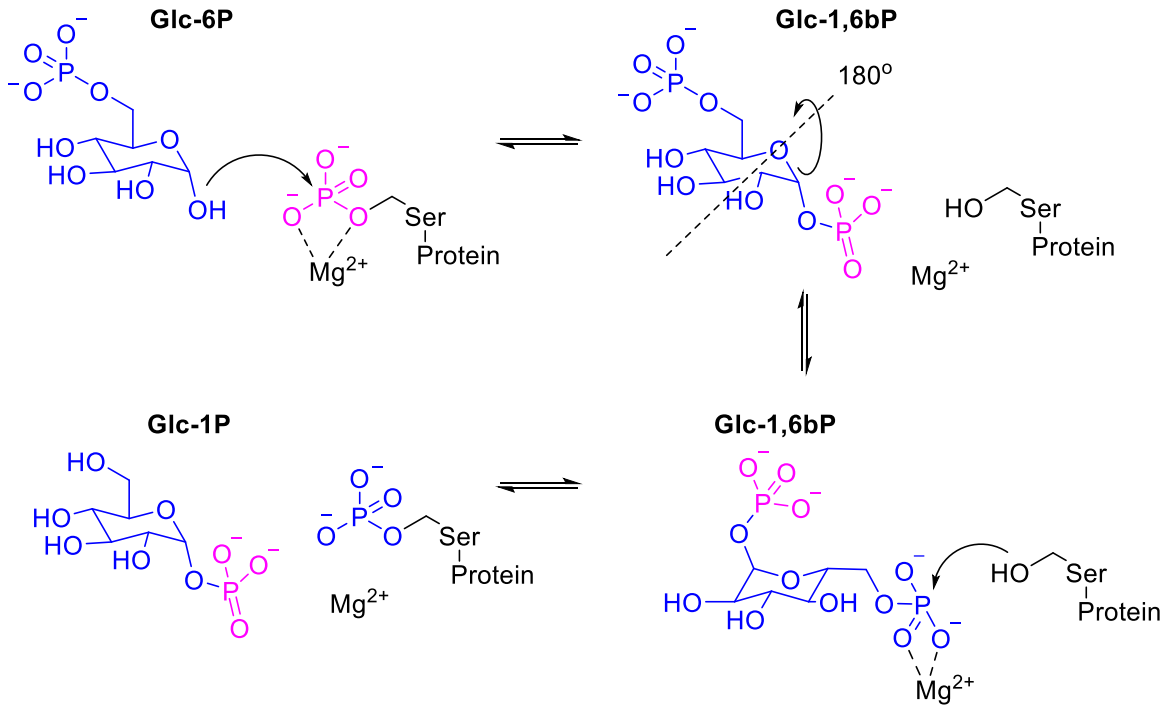

Figure 2 Simplified mechanism of Glc-6P and Glc-1P interconversion by PGM; catalytic serine residues in *Af*PGM S114, *Hs*PGM and *Ca*PGM S117. Glc-1P- glucose 1-phosphate, Glc-6P- glucose 6-phosphate, Glc-1,6bP- glucose 1,6-bisphosphate

Although the motion of domain IV (phosphoryl-recognising domain) is essential for catalytic activity[88], studies on *Pseudomonas aeruginosa* PGM suggest that domains I-III also move[90]. The change of domains I-III conformation is linked to stabilising the transition state (step 2), thus having a direct influence on the catalytic efficiency of the PGM enzyme[70].

*Af*PGM is located in the middle of the UDP-glucose pathway upstream of UGP and downstream of PGI (**Figure 1,** glucan pathway). UDP-glucose is an essential metabolite[91], and in the fungal cell wall context, UDP-Glc is a fundamental building block for β-1,3-glucan[53], α-1,3-glucan[92] and galactomannan[63]. Additionally, it is involved in trehalose biosynthesis, a disaccharide central to fungal metabolism and stress response[93] (**Figure 1,** violet pathway). Targeting the UDP-glucose biogenesis has the potential to disrupt not only multiple cell wall components but also the crucial trehalose metabolic pathway. Only two molecules were reported as potential mechanism-inspired inhibitors of phosphoglucomutases: xylose-1 phosphate and ribose-1 phosphate[94], with minor potential for developing selective inhibitors.

The high throughput fragment screening campaign yielded no promising hits for *Af*PGI and *Af*UGP (van Aalten unpublished). Contrastingly, the same screens against *Af*PGM and *Ca*PGM (a close *Candida albicans* orthologue of *Af*PGM) resulted in a discovery of a small thiol-reactive molecule 2-(3-chloro-2-fluorophenyl) isothiazol-3(2H)-one with an acronym ISFP1 (Isothiazolone Fragment of PGM 1). The hit fragment exhibited a low micromolar inhibition towards both fungal enzymes[95]. As ISFP1 carries

an isothiazolone warhead, thus its inhibitory mode was assumed as covalent[96], later confirmed by mass spectrometry[70]. The intact mass spectrometry of the reaction between *Af*PGM$_{WT}$ and ISFP1 in a 1: 20 ratio revealed a mass shift of 232 Da compared to the unmodified protein corresponding to a mass of a single ISFP1 adduct (exact mass: 229.98 Da) per one *Af*PGM molecule.

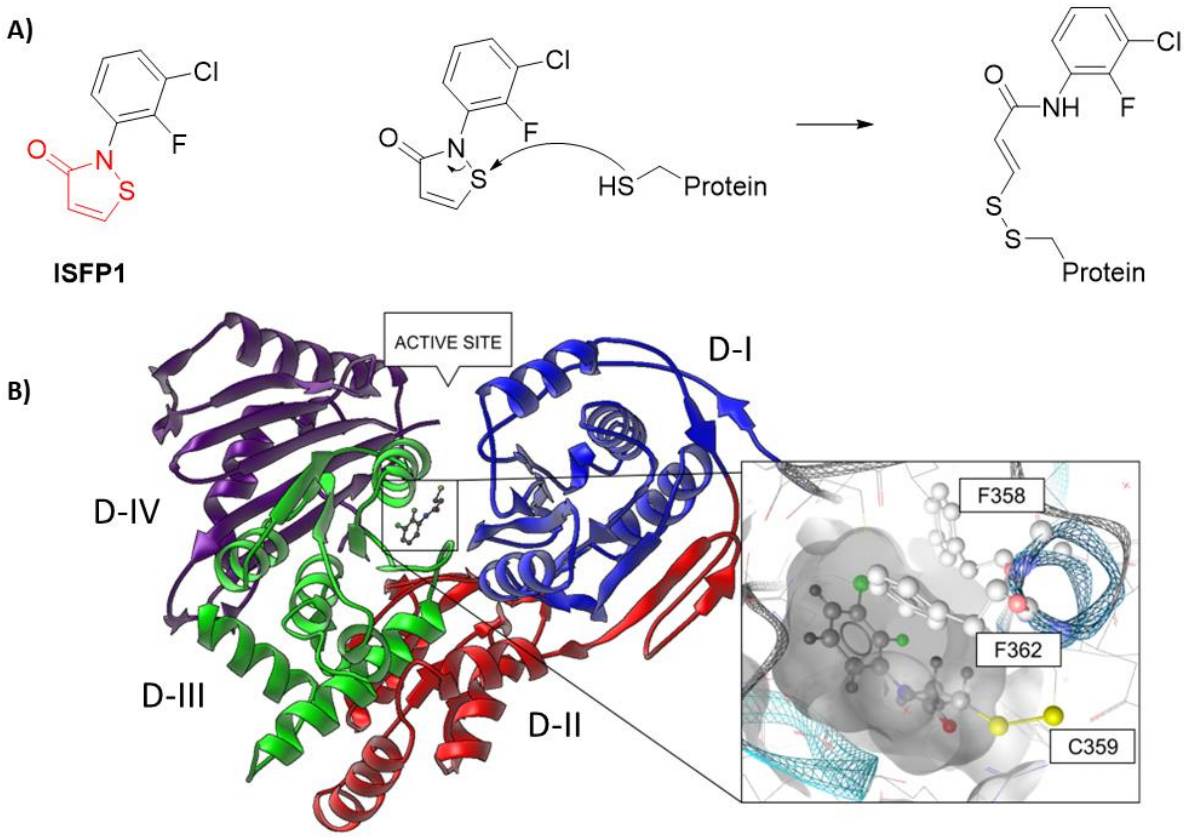

Figure 3 Interaction of ISFP1 with target proteins. Panel **A)**, the structure of ISFP1 (red isothiazolone warhead) and mechanism of disulphide bond formation; Panel **B)**, experimental co-crystal structure of *Ca*PGM with ISFP1 (PDB entry: 7PJC) with a close-up on the ISFP1 induced pocket. PGM domains are highlighted in different colours, blue- domain I, red- domain II, green- domain III and violet- domain IV.

The *Af*PGM hit fragment, ISFP1, is considered a pan-assay interference compound (PAIN)[96–98]. ISFP1 carries a thiol-reactive warhead forming disulphide bonds (**Figure 3A**) and might interact with its protein targets in a non-drug-like manner[96]. Typically, such molecules are discarded as false positives. However, some isothiazolone derivatives have found use as antimicrobials[99]. Working with PAINs compounds requires extreme caution and a systematic approach. The only reason why ISFP1 was of any interest for further investigation was its co-crystal structure with *Af*PGM's close orthologue *Ca*PGM (**Figure 3B**). The co-crystal structure of *Ca*PGM revealed the modification site to be a cysteine (C359) in an induced pocket at the interface of domains I-III[95]. Interestingly, the pocket formation results from tryptophan 355 flipping to the protein's surface, and the motion of W355 is the only

noticeable change in protein conformation[70]. Moreover, C359 (**Figure 4**, C359 highlighted with a violet star) is not conserved in human phosphoglucomutase but is conserved among fungal PGMs, including *Af*PGM (C353). *Af*PGM and *Ca*PGM share 66% protein sequence identity and both fungal enzymes share 55% and 54% sequence identity with the human orthologue, *Hs*PGM. Moreover, active serine magnesium binding and the phosphate binding motifs are highly conserved among all three orthologues (**Figure 4**).

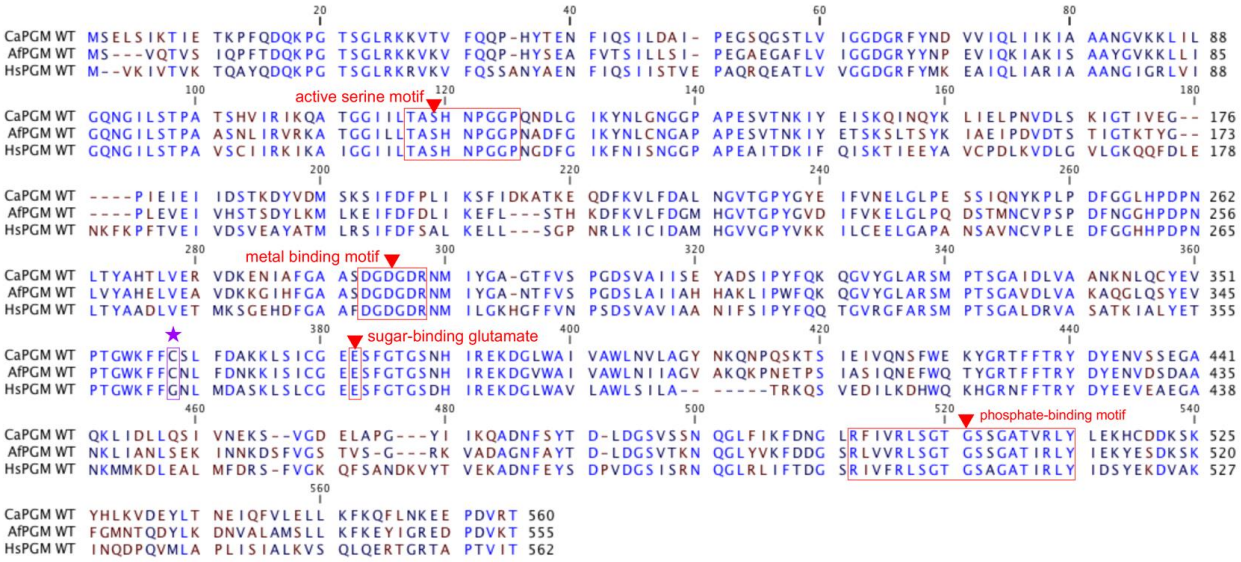

Figure 4 Sequence alignment of PGM enzymes; Sequence identity of *Ca*PGM and *Af*PGM: 66%, *Ca*PGM and *Hs*PGM 54%, *Af*PGM and *Hs*PGM 55%; violet star indicates non-conserved cysteine C359 in *Ca*PGM and C353 in *Af*PGM. Blue residues indicate conservation among all three orthologues.

Aspergillus fumigatus PGM might be a promising target for novel antifungals as the enzyme has been genetically validated[70]. Although generating the *pgm* knockout stain was unsuccessful, replacing the native *Aspergillus fumigatus pgm* promoter with the alcohol dehydrogenase promoter (P_{alcA}) from *Aspergillus nidulans* yielded a strain (P_{alcA}*::pgm*) that could be tightly controlled by the presence of alcohol, glycerol and threonine[70]. P_{alcA}*::pgm* conditional mutant displayed a comparable growth to the wild-type on solid minimal media supplemented with ethanol, glycerol and threonine (100 mM)[70]. In contrast, on complete media and YEPD without supplementation with alcohols, the growth of the mutant strain was completely inhibited[70].

Although PGM in *Aspergillus fumigatus* is an essential enzyme and a non-conserved pocket/ residue has been identified by ISFP1[70,95], it is still unknown whether the enzyme inhibition is real. The isothiazolone hit fragment might not interact with PGM in a drug-like manner, possibly causing aggregation or protein precipitation rather than inhibition.

Project aims

Aspergillosis caused by *Aspergillus fumigatus* is a life-threatening disease, increasingly burdening immunocompromised and non-immunocompromised individuals. Over the last twenty years, no new drugs have been discovered to revolutionise aspergillosis treatment. Growing fungal resistance to current therapies may leave us defenceless against this opportunistic pathogen. Thus it is crucial to search for novel antifungal targets.

*Af*PGM is an essential enzyme participating in fungal cell wall biosynthesis. Preliminary data indicated that *Af*PGM might be covalently and selectively inhibited by the isothiazolone fragment (ISFP1) obtained from the high-throughput fragment screen. The isothiazolone hit fragment is an unreliable molecule often interacting with proteins in a non-drug-like manner, causing aggregation or precipitation. The interaction between *Af*PGM and ISFP1 raises several questions, and this work aims to answer them.

1. Is inhibition of *Af*PGM exclusively elicited via engagement of cysteine C353?
2. Is inhibition of *Af*PGM based on drug-like interactions between the enzyme and its fragment hit?
3. How does the engagement of cysteine C353 in *Af*PGM elicit inhibition?
4. Can a non-thiazolone-based molecule inhibit *Af*PGM via cysteine C353?

Methodology

Recombinant protein expression and purification of PGM proteins

Table M 1 List of primers used in this work

Description		Primers	Sequence (5' to 3')
Full-length *Af*PGM		P1	CTGGGATCC ATGTCGGTCCAGACGGTCTCCATTCAG
		P2	GATGCGGCCGC TTAAGTCTTGACATCAGGGTCCTCCCG
Full-length *Af*PGM		P3	CCGGCTGGAAGTTCTTCAGCAACCTCTTTGATAAC
C353S		P4	GTTATCAAAGAGGTTGCTGAAGAACTTCCAGCCGG
Full-length *Af*PGM		P5	CACCGGCTGGAAGTTCTTCGCCAACCTCTTTGATAACAAG
C353A		P6	CTTGTTATCAAAGAGGTTGGCGAAGAACTTCCAGCCGGTG
Full-length *Af*PGM		P7	CCGGCTGGAAGTTCTTCGGCAACCTCTTTGATAAC
C353G		P8	GTTATCAAAGAGGTTGCCGAAGAACTTCCAGCCGG
Full-length *Af*PGM		P9	CCCACCGGCTGGAAGTTCTTCGTGAACCTCTTTGATAACAAGAAG
C353V		P10	CTTCTTGTTATCAAAGAGGTTCACGAAGAACTTCCAGCCGGTGGG
Full-length *Af*PGM C353*	AfPGM_C131S_fwd	P11	GTATCAAGTACAACTTGAGCAATGGTGCCCCCGC
	AfPGM_C131S_rev	P12	GCGGGGGCACCATTGCTCAAGTTGTACTTGATAC
	AfPGM_C242S_fwd	P13	CAAGACAGCACCATGAACAGCGTCCCCAGCCCTGAC
	AfPGM_C242S_rev	P14	GTCAGGGCTGGGGACGCTGTTCATGGTGCTGTCTTG
	AfPGM_C364S_fwd	P15	GATAACAAGAAGATCTCCATCAGCGGTGAGGAGAGTTTCG
	AfPGM_C364S_rev	P16	CGAAACTCTCCTCACCGCTGATGGAGATCTTCTTGTTATC
Full-length *Ca*PGM		P17	AAAGGATCCATGTCAGAATTGTCAATCAAGACAATC
		P18	AAAGCGGCCGCTTACGTGCGTACGTCGGGTTCTTCC
Full-length *Ca*PGM		P19	CTGGCTGGAAGTTTTTCAGTTCTTTGTTTGACGCC
C359S		P20	GGCGTCAAACAAAGAACTGAAAAACTTCCAGCCAG
Full-length *Ca*PGM		P21	GCCTACTGGCTGGAAGTTTTTCGTGTCTTTGTTTGACGCCAAAAAGC
C353V		P22	GCTTTTTGGCGTCAAACAAAGACACGAAAAACTTCCAGCCAGTAGGC
Full-length *Hs*PGM		P23	CTGGGATCCATGGTGAAGATCGTGACAGTTAAGACC
		P24	GATGCGGCCGCTTAGGTGATGACAGTGGGTGCAGTGCG

Dr Andrew Farebnach performed cloning, and methods have been described extensively in a recent publication[70]. PCR products have been cloned into a 6His-tag modified version of pGEX6P1 (GE Healthcare).

All proteins have been expressed *E. coli* BL21 (DE3) pLysS cells.

Transformation

The appropriate plasmid (1 µL) was added to freshly thawed competent cells suspension (50 µL) and incubated on ice for 15 min. Then cell suspension was heat shocked at 42°C for 60 s and returned to the ice, followed by the addition of SOC medium (150 µL). The transformed cell suspension was incubated at 37 °C in an Infors shaker for 45 min, then plated on Luria-Bertani agar plates supplemented with carbenicillin (100 µg /mL or 2 x AMP) and left incubated overnight at 37 °C.

Recombinant protein expression

A single colony was picked, added to fresh Luria-Bertani (LB) broth supplemented with carbenicillin (100 µg /mL or 2 x AMP), and incubated overnight in the infors shaker at 37 °C. The starting culture was used to inoculate (5 mL) to a fresh LB 2 x AMP broths (1 L) and incubated at 37 °C until the optical density of the culture reached approximately 0.6, then the temperature of the incubator was lowered to 18 °C, and isopropyl β-d-1-thiogalactopyranoside (250 µL, 1 M) was added to each culture, then left incubated overnight at 18 °C.

Recombinant protein purification

After approximately 18 h incubation, cells were harvested by centrifugation, resuspended in HEPES-NaOH buffer with 150 mM NaCl at pH 7.5, and lysed using a French press (at 500 psi). The cell debris was separated by centrifugation (40 000g) for 30 min. The supernatant was collected and incubated with fresh Ni^{2+} beads (approx. 5 mL per 4 L of culture), equilibrated with HEPES-NaOH buffer with 150 mM NaCl at pH 7.5, for 1 hour at 4 °C. After 1 h incubation, the lysate was drained from Ni^{2+}-beads, followed by two washes with HEPES-NaOH buffer with 150 mM NaCl at pH 7.5, and three washes of HEPES-NaOH buffer with 150 mM NaCl at pH 7.5 containing increasing concentration of imidazole (20, 30 and 50 mM). Protein was eluted with 20 mL of HEPES-NaOH buffer with 150 mM NaCl at pH 7.5 containing 200 mM imidazole. Prescission Protease (4 mg /mL, 100 µL) was added to the protein elution, and the solution was transferred to the dialysis membrane and dialysed at 4 °C to a fresh HEPES-NaOH buffer with 150 mM NaCl at pH 7.5 overnight. Dialysed protein was then concentrated using a protein concentrator with a 20 kDa cut-off and loaded onto the 26/600 Superdex 75 prep-grade gel filtration column using HEPES-NaOH buffer with 150 mM NaCl at pH 7.5 as a mobile phase. All PGM proteins used in this work can be produced in very high yields (10-30 mg / culture litre) using this method.

Determination of Michaelis-Menten kinetics of PGM enzymes

The enzymatic activity of recombinantly expressed phosphoglucomutases was determined using glucose-6-phosphate dehydrogenase from *Leuconostoc mesenteroides* (*Lm*G6PDH) coupled assay (**Scheme M1**). Glucose-1,6-bisphosphate (G1,6bP) was used to phosphorylate the enzyme. Glucose-1-phosphate (G1P) was utilised as a substrate that PGM converted to glucose-6-phosphate (G6P). *Lm*G6PDH would then oxidise G6P to 6-phosphogluconolactone, reducing $NADP^+$ to NADPH which gave a fluorescence signal.

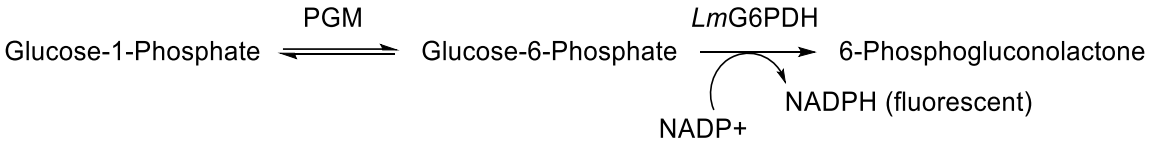

Scheme M 1 General scheme of phosphoglucomutases enzyme assays. PGM enzymes interconvert G1P and G6P. In the presence of glucose-6-phosphate dehydrogenase and $NADP^+$, G6P is oxidised to 6-phosphogluconolactone and $NADP^+$ is reduced to fluorescent NADPH. The fluorescence signal is proportional to the production of G6P.

All assays have been formatted to 96-well plates. Fluorescence readings were taken using a SpectraMax I3 plate reader.

Buffer A = MOPS 50 mM and $MgSO_4$ 1.5 mM, pH 7.4

Reaction mixture = *Lm*G6PDH (0.004 u/µL), NADP+ (40 mM) and G1,6bP (2 mM) in Buffer A

Experiments were performed in 96-well black plates. Glucose-1-phosphate (10 µL, 60 mM, 20 mM, 6.6 mM, 2.2 mM, 0.74 mM, 0.24 mM and 0.08 mM) in buffer A was added to appropriate wells (**Figure M1**) in triplicate, followed by the addition of **Buffer A** (70 µL) to experimental wells and **Buffer A** (80 µL) to baseline wells. A **reaction mixture** (10 µL) was added to those solutions, followed by PGM enzyme (10 µL, 50 nM) addition to experimental wells. Solutions were briefly mixed, and their fluorescence was taken by the plate reader at excitation wavelength 360 nm and emission 460 nm for 10 min, every 30 s at room temperature. The raw data was processed in Prism. The background signal was subtracted from the experimental signal, and the readings were converted to NADPH concentration using the standard curve. Then, the velocity of NADPH within the first two minutes of the assay was plotted against G1P concentration. Curves were fitted using the standard Michaelis-Menten model in Prism 8.

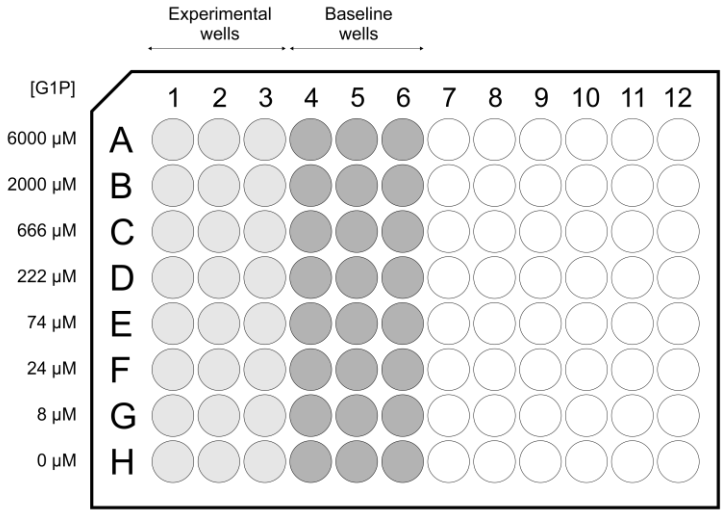

Figure M 1 General plate layout of PGM enzyme assays

PGM Inhibitory assays

Time-independent assays

All assays have been formatted to 96-well plates. Fluorescence readings were taken using a SpectraMax I3 plate reader.

Buffer A = MOPS 50 mM and $MgSO_4$ 1.5 mM, pH 7.4

Reaction mixture 2 = *Lm*G6PDH (0.004 u/µL), $NADP^+$ (40 mM), G1,6bP (2 mM) and G1P (20 mM) in **Buffer A**

Experiments were run in a black 96-well plate. ISFP1 (10 µL, 4 mM, 1 mM, 0.25 mM, 0.0625 mM, 0.015 mM and 0.004 mM) in **Buffer A** was added to appropriate wells (**Figure M2**) in triplicate, followed by the addition of **Buffer A** (70 µL) to experimental wells and **Buffer A** (80 µL) to baseline wells. A **reaction mixture 2** (10 µL) was added to those solutions, followed by PGM enzyme (10 µL, 50 nM) addition to experimental wells. Solutions were briefly mixed, and their fluorescence was taken by the plate reader at excitation wavelength 360 nm and emission 460 nm for 30 min, every 60 s at room temperature. The raw data was processed in Prism. The background signal was subtracted from the experimental signal, and the raw inhibitory data were normalised over the enzymatic activity of the uninhibited enzyme. The uninhibited enzyme served as 100% of the PGM activity. Relative activities at 5 min timepoint (linear range, below 10% substrate consumption) were plotted against the ISFP1 concentration and fitted to the standard (built-in) dose-response inhibition model with four variable parameters in Prism 8 without constricting the top and bottom range.

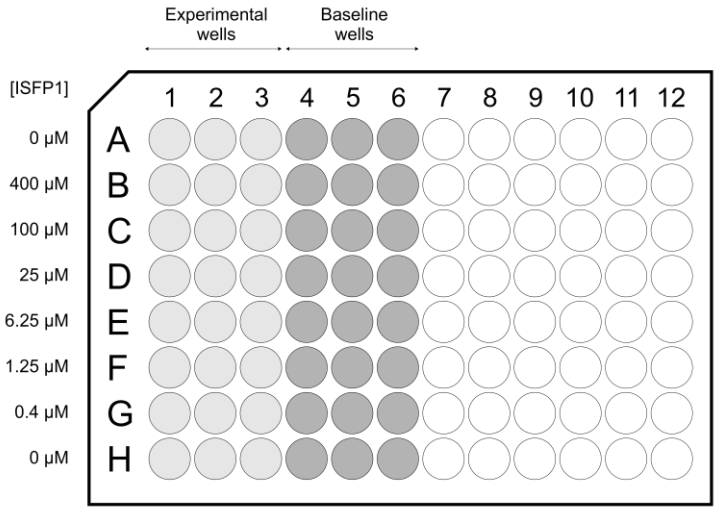

Figure M 2 General layout of the time-independent inhibitory assay.

Time-dependent assays

All assays have been formatted to 96-well plates. Fluorescence readings were taken using a SpectraMax I3 plate reader.

Buffer A = MOPS 50 mM and $MgSO_4$ 1.5 mM, pH 7.4

Reaction mixture 2 = *Lm*G6PDH (0.004 u/µL), NADP+ (40 mM), G1,6bP (2 mM) and G1P (20 mM) in **Buffer A**

N-phenyl maleimide (NPM) experiments were run only with 30 min pre-incubation period

Experiments were run in a black 96-well plate. ISFP1/NPM (10 µL, 4 mM, 1 mM, 0.25 mM, 0.0625 mM, 0.015 mM and 0.004 mM) in **Buffer A** was added to appropriate wells (**Figure M3**) in triplicate, followed by the addition of **Buffer A** (70 µL) to experimental wells and **Buffer A** (80 µL) to baseline wells. **Reaction mixture 2** (10 µL) was added to columns 10-12 (baseline wells). A PGM solution (10 µL, 50 nM) was added to columns 7-9, then 10 min later to 4-6 and 5 min later to 1-3 (**Figure M3**), followed by the immediate addition of a **reaction mixture 2** (10 µL) addition to all experimental wells. Solutions were briefly mixed, and their fluorescence was taken by the plate reader at excitation wavelength 360 nm and emission 460 nm for 30 min, every 60 s at room temperature. The raw data was processed in Prism. The background signal was subtracted from the experimental signal, and the inhibitory data were normalised over the enzymatic activity of the uninhibited enzyme. The uninhibited enzyme served as 100% of the PGM activity. Relative activities at five minutes timepoint (linear range, below 10% substrate consumption) were plotted against the ISFP1 concentration and fitted to the standard (built-in) dose-response inhibition model in Prism 8 with four variable parameters without constricting the top and bottom range.

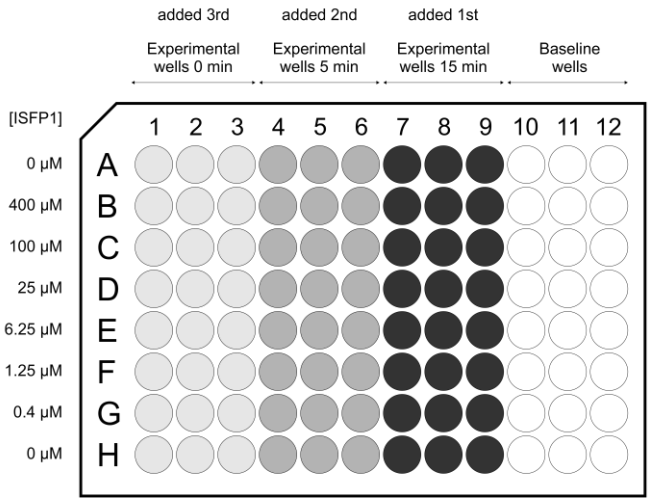

Figure M 3 General layout of the time-dependent inhibitory assay.

DTT rescue experiment

All assays have been formatted to 96-well plates. Fluorescence readings were taken using a SpectraMaxI3 plate reader.

Buffer A = MOPS 50 mM and $MgSO_4$ 1.5 mM, pH 7.4

Reaction mixture 2 = *Lm*G6PDH (0.004 u/µL), NADP+ (40 mM), G1,6bP (2 mM) and G1P (20 mM) in **Buffer A**

Experiments were run in a black 96-well plate. ISFP1 (10 µL, 500 µM) in **Buffer A** was added to appropriate wells (**Figure M4**) in triplicate, followed by the addition of **Buffer A** (60 µL) to experimental wells and **Buffer A** (70 µL) to baseline wells. **Reaction mixture 2** (10 µL) was added to columns 10-12 (baseline wells), and DTT Solution (10 µL, 100 mM) in **Buffer B** was added to columns 7-9 (**Figure M4**). *Af*PGM and *Hs*PGM (10 µL, 50 nM) were added to the experimental wells and left for 15 min pre-incubation with ISFP1. After a pre-incubation period, DTT (10 µL, 100 mM) was added to columns 1-3, and **reaction mixture 2** was added to all remaining wells. Solutions were briefly mixed, and their fluorescence was taken by the plate reader at excitation wavelength 360 nm and emission 460 nm for 15 min, every 60 s at room temperature. The raw data was processed in Prism. The background signal was subtracted from the experimental signal, and the readings were normalised over the uninhibited enzyme and plotted without further processing

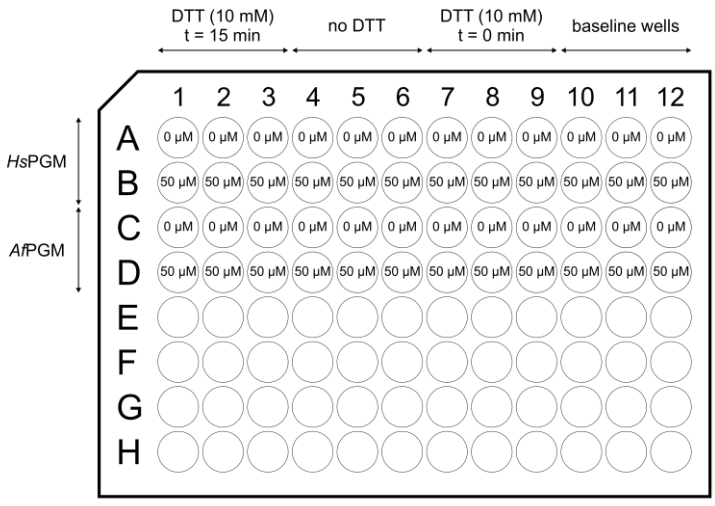

Figure M 4 General layout of the DTT rescue experiment

Mechanism of action experiments

All assays have been formatted to 96-well plates. Fluorescence readings were taken using a SpectraMax I3 plate reader.

Buffer A = MOPS 50 mM and $MgSO_4$ 1.5 mM, pH 7.4

Reaction mixture 2 = *Lm*G6PDH (0.004 u/µL), NADP+ (40 mM), G1,6bP (2 mM) and G1P (variable). Five separate experiments were performed, each at different Glucose-1-phosphate concentrations: [G1P]= 0.560 mM, 1.12 mM, 2.24 mM, 4.48 mM and 8.96 mM

Experiments were run in a black 96-well plate. ISFP1 (10 µL, 200 µM, 100 µM, 50 µM, 25 µM, 12.5 µM and 6.25 µM and 3.15 µM) in **Buffer A** was added to appropriate wells **(Figure M5**) in triplicate, followed by the addition of **Buffer A** (70 µL) to experimental wells and **Buffer A** (80 µL) to baseline wells. A **reaction mixture 2** (10 µL) was added to those solutions, followed by *Af*PGM enzyme (10 µL, 20 nM) addition to experimental wells. Solutions were briefly mixed, and their fluorescence was taken by the plate reader at excitation wavelength 360 nm and emission 460 nm for 30 min, every 60 s at room temperature. The raw data was processed in Prism. The background signal was subtracted from the experimental signal, and the readings were converted to NADPH concentration using the standard curve. Then, the velocity of NADPH within the first two minutes of the assay was plotted against G1P. Curves were fitted using the standard Michaelis-Menten model in Prism 8.

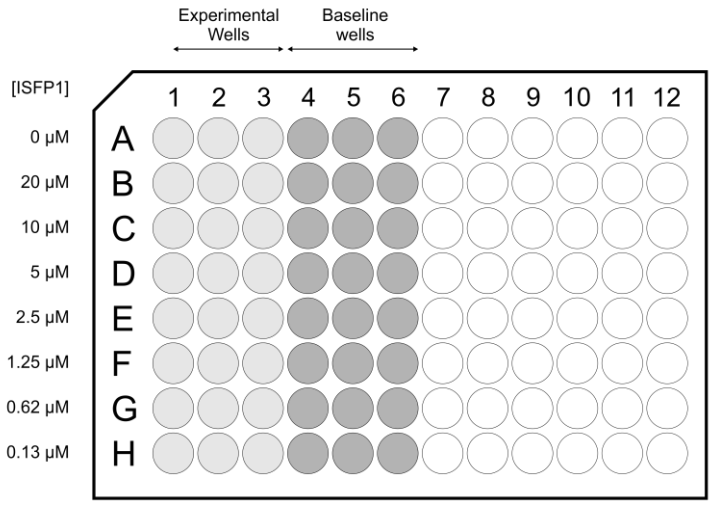

Figure M 5 General layout of mechanism of action experiments

Mass spectrometry experiments

To a solution of recombinantly expressed triple cysteine mutein (C124S, C242S and C364S) *Af*PGM$_{C353*}$ (200 µL, 20 µM) in MOPS 50 mM and $MgSO_4$ 1.5 mM, pH 7.4, *N*-Phenyl maleimide (0.4 µL, 100 mM) in DMSO was added. The solution was left at room temperature for 30 min, then transferred to the dialysis membrane and dialysed into fresh MOPS 50 mM and $MgSO_4$ 1.5 mM, pH 7.4 for 8 h at 4 ^{O}C. The dialysed sample was run on 6130 Quadruple LC/MS instrument from Agilent Technologies (Santa Clara, US), using ZORBAX 300SB-C3 5 µm column, with acetonitrile and water (ACN: H_2O) gradient from 10: 90% to 95: 5% over 30 min. The intact mass spectrometry was deconvoluted using built-in Agilent software.

To a solution of recombinantly expressed *Af*PGM$_{C353V}$ (200 µL, 20 µM) in MOPS 50 mM and $MgSO_4$ 1.5 mM, pH 7.4, *N*-Phenyl maleimide (0.4 µL, 100 mM) in DMSO was added. The solution was left at room temperature for 30 min, then transferred to the dialysis membrane and dialysed into fresh MOPS 50 mM and $MgSO_4$ 1.5 mM, pH 7.4 for 8 h at 4 ^{O}C. The dialysed sample was run on 6130 Quadruple LC/MS instrument from Agilent Technologies (Santa Clara, US), using ZORBAX 300SB-C3 5 µm column, with acetonitrile and water (ACN: H_2O) gradient from 10: 90% to 95: 5% over 30 min. The intact mass spectrometry was deconvoluted using built-in Agilent software.

To a solution of recombinantly expressed triple cysteine mutein (C124S, C242S and C364S) *Af*PGM$_{C353*}$ (200 µL, 20 µM) (negative control) in MOPS 50 mM and $MgSO_4$ 1.5 mM, pH 7.4, DMSO (0.4 µL) was added. The solution was left at room temperature for 30 min, then transferred to the dialysis membrane and dialysed into fresh MOPS 50 mM and $MgSO_4$ 1.5 mM, pH 7.4 for 8 h at 4 ^{O}C. The dialysed sample was run on 6130 Quadruple LC/MS instrument from Agilent Technologies (Santa Clara, US), using ZORBAX 300SB-C3 5 µm column, with acetonitrile and water (ACN: H_2O) gradient from 10: 90% to 95: 5% over 30 min. The intact mass spectrometry was deconvoluted using built-in Agilent software.

To a solution of recombinantly expressed *Af*PGM$_{C353V}$ (200 µL, 20 µM) (negative control) in MOPS 50 mM and $MgSO_4$ 1.5 mM, pH 7.4, DMSO (0.4 µL) was added. The solution was left at room temperature for 30 min, then transferred to the dialysis membrane and dialysed into fresh MOPS 50 mM and $MgSO_4$ 1.5 mM, pH 7.4 for 8 h at 4 ^{O}C. The dialysed sample was run on 6130 Quadruple LC/MS instrument from Agilent Technologies (Santa Clara, US), using ZORBAX 300SB-C3 5 µm column, with acetonitrile and water (ACN: H_2O) gradient from 10: 90% to 95: 5% over 30 min. The intact mass spectrometry was deconvoluted using built-in Agilent software.

CPM Binding Assay

All assays have been formatted to 96-well plates. Fluorescence readings were taken using a SpectraMaxI3 plate reader.

Buffer B: HEPES-NaOH buffer with 150 mM NaCl at pH 7.4

In a black 96-well plate, NPM (20 µL, 1.3 mM, 0.4 mM, 0.14 mM, 0.04 mM, 0.016 mM, 0.005 mM and 0.0017 mM) was added to wells in column 12 (**Figure M6**), followed by **Buffer B** (170 µL) and *Af*PGM$_{C353*}$ (10 µL, 200 µM). The mixtures were left at room temperature for 60 min. Once the pre-incubation started, NPM (20 µL, 13 µM, 4.3 µM, 1.4 µM, 0.48 µM, 0.16 µM, 0.05 µM and 0.017 µM) was added to wells in columns 4-6 **(Figure M6**) followed by **Buffer B** (160 µL). **Buffer B** (178 µL) was also added to experimental wells in columns 1-3. Before the end incubation period, a thiol-reactive fluorophore, 7-Diethylamino-3-(4'-Maleimidylphenyl)-4-Methylcoumarin (CPM) (20 µL, 200 µM) in 50/50 **Buffer B** and DMSO was added to baseline and experimental wells (**Figure M6**). After 60 minutes of pre-incubation, samples from wells in column 12 (2 µL) were added to experimental wells in columns 1-3. Samples were briefly mixed, and their fluorescence readings were taken by the plate reader at excitation wavelength 384 nm and emission 470 nm for 90 min. The raw data was processed in Prism. The background signal was subtracted from the experimental signal, and the readings were plotted as a function of CPM fluorescence against time without fitting any model.

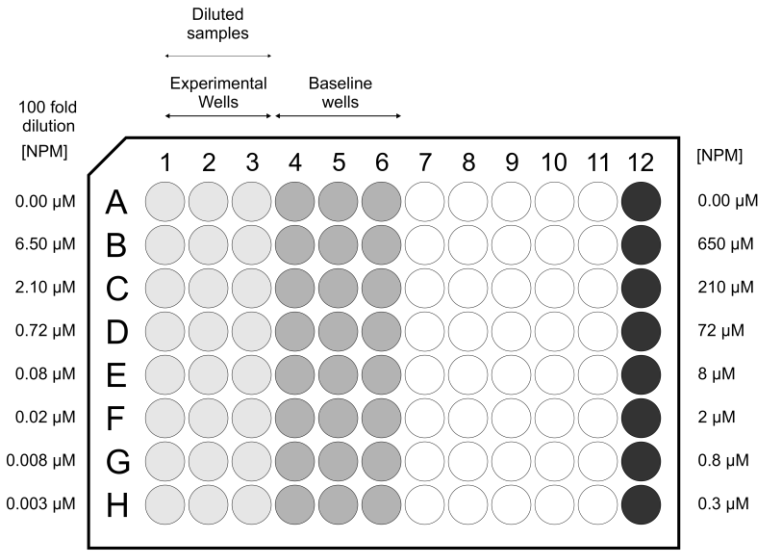

Figure M 6 General plate layout for the CPM binding assay.

Results

Cysteine 353 is not required for catalytic efficiency of *Af*PGM

To dissect the interaction between ISFP1 and *Af*PGM, several phosphoglucomutase enzymes were recombinantly expressed in *E.coli* (Table 1) and purified using His-GEX affinity purification via Ni^{2+} beads and size exclusion (**Figure 5**). Although *Af*PGM harbours four cysteines, preliminary data indicated that inhibition of *Af*PGM occurs via cysteine C353[95]. Substitution of cysteine C353 to different amino acids was necessary to generate a control mutein incapable of forming a disulphide bond[100] with ISFP1 at position 353, possibly abolishing *Af*PGM inhibition. Additionally, it was unknown if C353 residue in *Af*PGM is critical in the interconversion of glucose-1-phosphate and glucose-6-phosphate.

*Af*PGM mutein harbouring only one cysteine (353) was an indispensable tool for assessing the exclusiveness of cysteine C353 in *Af*PGM covalent inhibition.

*Hs*PGM was recombinantly expressed to determine if ISFP1 exhibits any selectivity towards fungal orthologue. Additionally, biochemical parameters were previously reported for human orthologue[101], and the protein was also utilised to validate the design of enzymatic assays.

Recombinantly expressed enzymes had to be biochemically active to give comparable results in inhibitory assays. Their enzymatic activity was determined by Glucose-6-phosphate-dehydrogenase coupled assay, using glucose-1-phosphate (G1P) as substrate (from 2 mM to 8 µM in three-fold dilution) and $NADP^+$ at a fixed 1 mM concentration. The NADPH, a product of $NADP^+$ reduction, served as a fluorescence reporter (**Scheme 1**). The fluorescence signal was then converted to NADPH concentration using a standard curve (**Figure 6**). The NADPH signal did not exhibit significant inner filter effects (self-quenching of fluorescence signal[102]) up to 125 µM, indicated by a very good linear fit of the fluorescence calibration curve with $R^2 = 0.9955$.

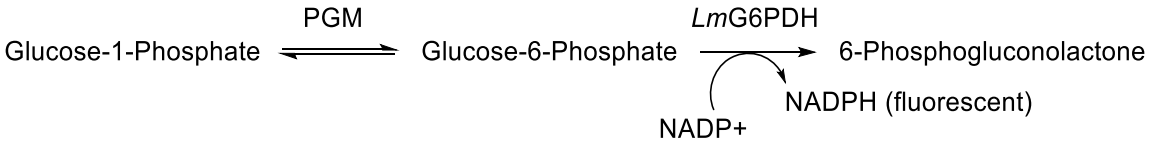

Scheme 1 General scheme of phosphoglucomutase enzyme assays. PGM enzymes interconvert glucose-1-phosphate and glucose-6-phosphate. In the presence of glucose-6-phosphate dehydrogenase and $NADP^+$, Glc-6-P is oxidised to 6-phophogluconolactone, and $NADP^+$ is reduced to fluorescent NADPH. The fluorescence signal is proportional consumption of Glc-6-P.

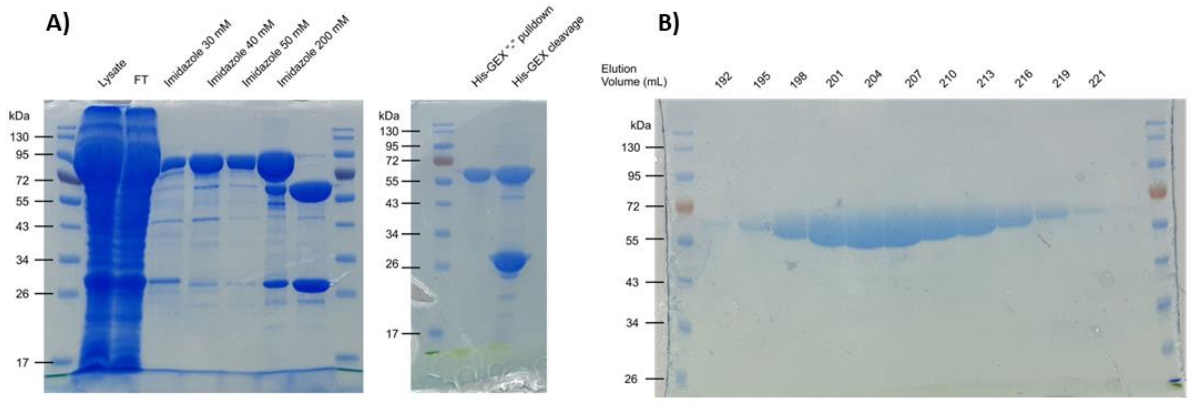

Figure 5 Representative SDS-PAGE gels (10%) of *Af*PGM$_{WT}$ (M_W *Af*PGM 61 kDa) purification using a combination of affinity purification and size exclusion. Panel **A)** initial purification using affinity beads (Ni^{2+}), FT – beads flow-through; **B)** size exclusion purification using 26/600 Superdex 75 prep-grade gel filtration column.

Using standard Michaelis-Menten models in Prism, the kinetic properties (K_m and k_{cat}) were obtained by globally fitting NADPH production velocity against glucose-1-phosphate concentration (Figure X). Velocities were determined within the first 2 min, and fluorescence readings were taken every 30 s. The consumption of substrate, glucose-1-phosphate, was below 10%.

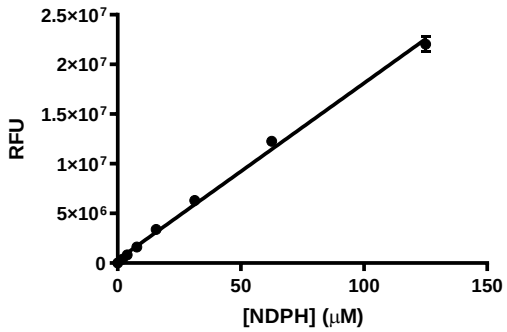

Figure 6 [NADPH] vs fluorescence calibration curve. Linear regression equation: Y= 177775x + 339691, with goodness of fit: R^2 = 0.9955. No significant inner filter effects were indicated up to 125 µM of NADPH. Error bars are standard deviations with three determinations.

Recombinantly expressed *Hs*PGM exhibited very similar values of K_m and k_{cat} to those previously reported[101] (**Table 1**, position 10, **Figure 7C**), validating the assay design.

Mutation of cysteine to serine is usually used to prevent cysteine-specific covalent modifiers from binding protein[103]. Attempts to generate *Af*PGM C353 mutation to serine resulted in an inactive enzyme (**Table 1** position 2). Initially, it was assumed that C353 might be an essential residue for *Af*PGM enzymatic activity. To determine if the same property occurs across other fungal PGMs, a mutein *Ca*PGM$_{C359S}$ was recombinantly expressed. Surprisingly, the substitution of *Ca*PGM$_{C359S}$

produced a fully functional enzyme (**Table 1**, position 8, **Figure 7B**), exhibiting similar kinetic properties to *Ca*PGM$_{WT}$ (**Table 1**, position 7, **Figure 7B**).

Three more *Af*PGM C353 muteins were recombinantly expressed and tested, including cysteine to alanine (**Table 1**, position 3), cysteine to glycine (**Table 1**, position 4) and cysteine to valine. Only *Af*PGM$_{C353V}$ was enzymatically active (**Table 1**, position 5, **Figure 7A**) and possessed K_m and k_{cat} values similar to *Af*PGM$_{WT}$ (**Table 1**, position 1).

Generating *Af*PGM$_{C353*}$, which harbours only one cysteine (C353), was less laborious. Substitution of cysteines 131, 242 and 364 to serines yielded an enzymatically active enzyme (**Table 1**, position 6, **Figure 7A**).

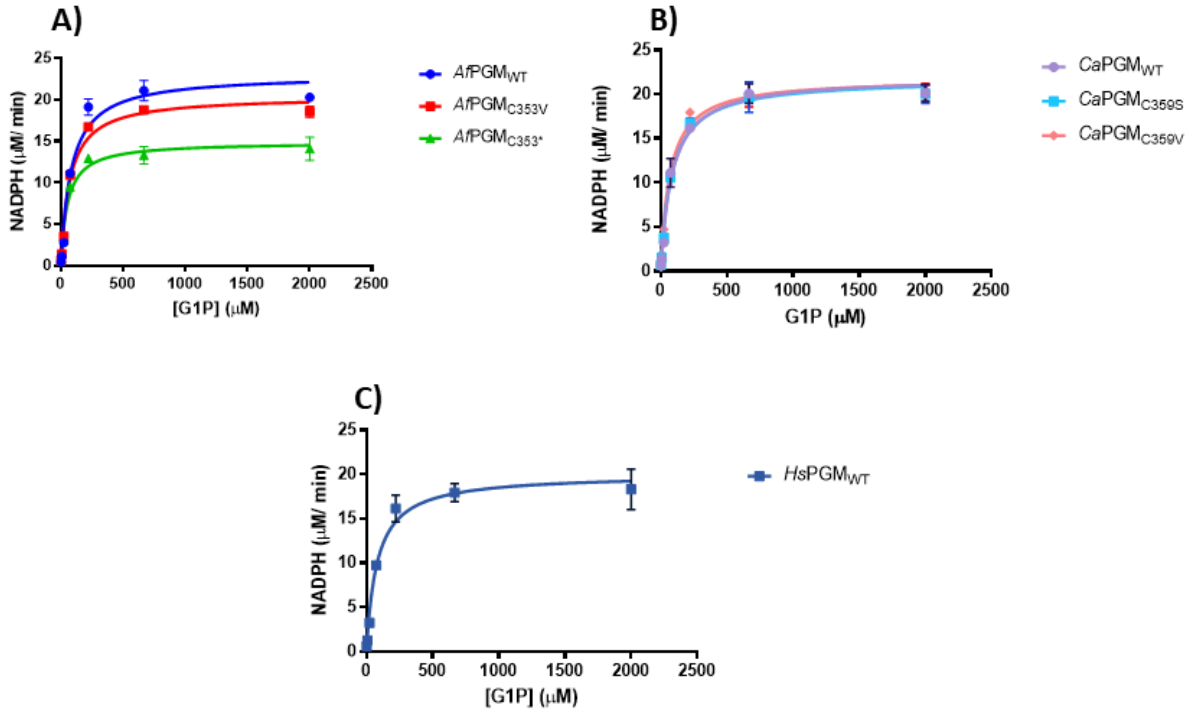

Figure 7 Michelis-Menten curves of recombinantly expressed PGM enzymes. Panel **A)** *Af*PGM WT and its C353 muteins; Panel **B)** *Ca*PGM WT and its C359 muteins, panel **C)** *Hs*PGM WT. Numeric values have been summarised in **Table 1**. Error bars are standard deviations with three determinations.

Table 1 Kinetic properties of recombinantly expressed phosphoglucomutases and their muteins. K_m Michaelis-Mentent constant; V_{max} enzyme's maximal velocity; k_{cat} turnover rate, k_{cat}/K_m enzymatic efficiency

	Enzyme	Mutation	K_m (μM)	V_{max} (μM s^{-1})	k_{cat} (s^{-1})	k_{cat}/K_m (μM^{-1} s^{-1})
1	*Af*PGM$_{WT}$	-	45 ± 6	0.49 ± 0.01	98	2.14
2	*Af*PGM$_{C353S}$	C353S	N/A[a]	N/A[a]	N/A[a]	N/A[a]
3	*Af*PGM$_{C353A}$	C353A	N/A[a]	N/A[a]	N/A[a]	N/A[a]
4	*Af*PGM$_{C353G}$	C353G	N/A[a]	N/A[a]	N/A[a]	N/A[a]
5	*Af*PGM$_{C353V}$	C353V	47 ± 5	0.39 ± 0.01	78	1.66
6	*Af*PGM$_{C353*}$	C131S, C242S, C364S	33 ± 5	0.26 ± 0.01	52	1.55
7	*Ca*PGM$_{WT}$	-	21 ± 3	0.48 ± 0.01	96	4.39
8	*Ca*PGM$_{C359S}$	C359S	18 ± 2	0.44 ± 0.01	88	4.88
9	*Ca*PGM$_{C359V}$	C359V	57 ± 7	0.57 ± 0.02	114	1.99
10	*Hs*PGM$_{WT}$	-	57 ± 7 (80 ± 4)[b]	0.57 ± 0.02	114 (143)[b]	1.97

[a] inactive enzyme, [b] reference values[101]

Substituting cysteine 353 in *Af*PGM for valine is unusual, however, it proves that C353 is not required for catalytic efficiency in *Aspergillus fumigatus* phosphoglucomutase 1. The reasoning behind inactive serine, alanine and glycine muteins could be only speculated, as the biological function of C353 is still unknown. Assuming C353 as a structural residue, not a nucleophilic thiolate, one could compare atomic radii of alanine, glycine, and serine with cysteine. The sulphur atom in cysteine residue has a larger atomic radius than oxygen in serine and methyl moiety in alanine. Therefore, substituting C353 might impact the overall structure, creating a "void" in the overall structure. Conversely, valine, having an isopropyl moiety, may mimic the thiol radius better than hydroxyl or methyl.

Cysteine 353 is required for inhibition of *Af*PGM with ISFP1

To determine if cysteine C353 in *Af*PGM was a target for ISFP1, recombinantly expressed wild-type enzyme and two muteins *Af*PGM$_{C353*}$ and *Af*PGMC$_{353V}$ were tested in inhibitory assays. Differences in the ISFP1 potency toward each protein indicated if C353 is an exclusive target of ISFP1.

The inhibitory assays were based on the enzymatic assays previously described (**Scheme 1**), with minor modifications of the substrate, fixed at a constant 500 µM (approx. 10 x K_m). Enzymes were added to a solution of assay components (NADP$^+$, *Lm*G6PDH and G1P) and ISFP1 at various concentrations (400 µM to 0.09 µM, in four-fold dilutions), referred to as time-independent assays. The time-dependent assays consisted of pre-incubation of *Af*PGM and muteins with ISFP1 for the indicated period (in parentheses on graphs), followed by adding assay components (NADP$^+$, *Lm*G6PDH and G1P).

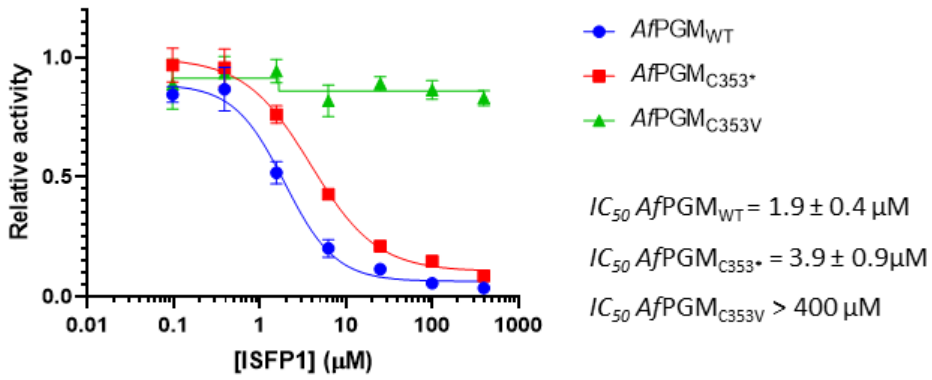

Figure 8 Time-independent inhibitory assays of ISFP1 against AfPGM (IC_{50} 2 µM), *Af*PGM$_{C353*}$ (IC_{50} 4 µM), and *Af*PGM$_{C353V}$ with no observable inhibition up to 400 µM ISFP1. Relative activity is the normalised result over the uninhibited enzyme, set as 100% activity. Error bars are standard deviations with three determinations.

In the time-independent inhibitory assays, ISFP1 displayed very similar potency against *Af*PGM$_{WT}$ and *Af*PGM$_{C353*}$ with IC_{50} of 2 µM and 4 µM, respectively (**Figure 8,** blue circles and red squares). On the other hand, *Af*PGM$_{C353V}$ does not experience significant inhibition up to 400 µM of ISFP1 (**Figure 8**, Green triangles), clearly indicating ISFP1 preference for C353.

The lack of *Af*PGM$_{C353V}$ inhibition also showed that glucose-6-phosphate dehydrogenase (*Lm*G6PDH), used in this assay to generate NADPH and the fluorescence, was not inhibited by ISFP1.

ISFP1 is a covalent modifier, and the binding equilibria of covalent inhibitors are time-dependent[104]. Their kinetic mechanisms vary between reversible and irreversible warheads. Although time-independent assays show similar half-maximal potency of ISFP1 towards wild-type and C353* enzymes and almost no inhibition towards *Af*PGM$_{C353V}$, an IC$_{50}$ does not account for changes over time. A more appropriate approach would be a determination of k_{inact}/K_i [105]. This rate constant describes the efficiency of the covalent bond resulting from the molecule's potency in the first binding step (K_i) and the maximum rate of the inactivation k_{inact} (rate of the covalent bond formation)[106]. Several attempts were made to determine k_{inact} and K_i parameters using direct extraction from inhibitory assays. However, due to technical difficulties, no proper method was devised.

To avoid the complexities of generating k_{inact} and K_i values, analysis of time-dependent IC$_{50}$ shifts was used. *Af*PGM$_{WT}$ and *Af*PGM$_{C353V}$ were pre-incubated with ISFP1 at variable concentrations (400 µM to 0.09 µM, in four-fold dilutions) and for three periods 0 min, 5 min and 15 min. The stability of PGM enzymes at room temperature at low concentrations (up to 5 nM) depends on the mutation and the recombinant protein origin. Although *Af*PGM and its muteins are generally stable at room temperature for up to 20-30 min, *Hs*PGM is very unstable and loses its enzymatic activity after prolonged experiments (more than 15-20 min). For consistency, if not stated otherwise, experiments were performed within the stability window of *Hs*PGM.

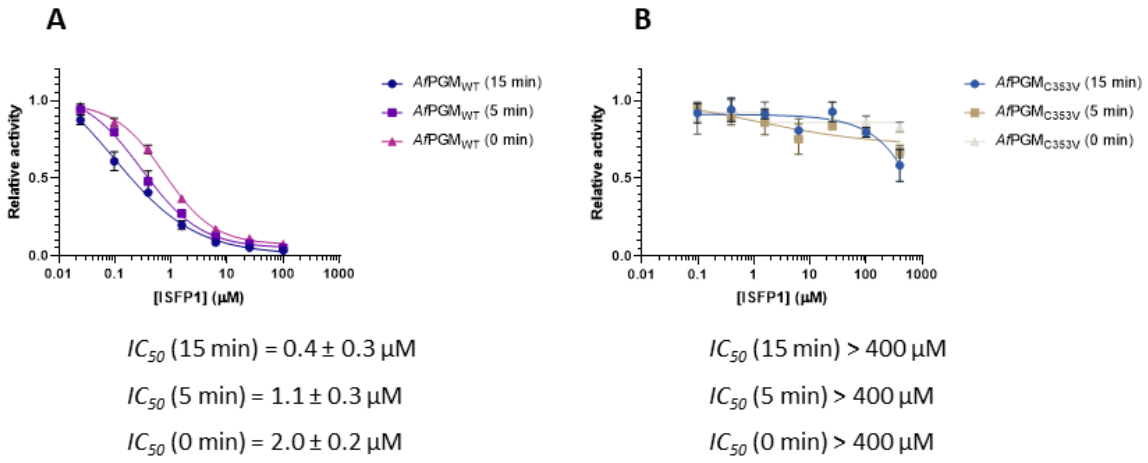

Figure 9 Time-dependant IC$_{50}$ shifts of (**A**) *Af*PGM$_{WT}$ and (**B**) *Af*PGM$_{C353V}$. Pre-incubation of ISFP1 with *Af*PGM$_{WT}$ resulted in a five-fold increase in ISFP1 potency (from 2.0 µM to 0.4 µM). Pre-incubation of *Af*PGM$_{C353V}$ with ISFP1 caused only partial impairment of the enzyme at 400 µM of inhibitor after 15 min. Relative activity is the normalised result over the uninhibited enzyme, set as 100% activity. Error bars are standard deviations with three determinations.

Pre-incubation of *Af*PGM and *Af*PGM$_{C353V}$ with ISFP1 did not cause significant shifts in potency. The C353V mutein remained almost uninhibited, displaying only slight impairment at the highest

concentration of ISFP1, followed by 15 min pre-incubation (**Figure 9B**). Similarly, pre-incubation of ISFP1 with *Af*PGM$_{WT}$ increased its potency only five-fold, causing an IC_{50} shift from 2 µM to 0.4 µM (**Figure 9A**). Both time-dependent and time-independent experiments indicated that cysteine C353 in *Af*PGM is required to inhibit *Af*PGM by ISFP1.

ISFP1 does not display any preference toward *Af*PGM over *Hs*PGM

ISFP1 requires cysteine 353 to inhibit *Af*PGM, which is not conserved in human orthologue. However, *Hs*PGM harbours six cysteines potentially available for (aspecific) modification by ISFP1. To determine whether the isothiazolone exhibits selectivity towards fungal PGM, *Hs*PGM inhibition was assessed in a time-dependent assay.

Similarly to the time-dependent fungal PGM assay, *Hs*PGM was pre-incubated with ISFP1 for three periods, 0 min, 5 min and 15 min, at variable concentrations of ISFP1 (400 µM to 0.09 µM, in four-fold dilutions).

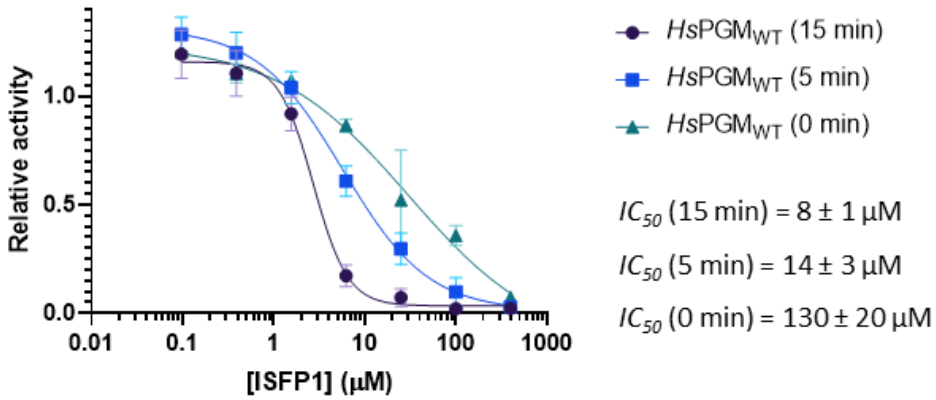

Figure 10 Time-dependent inhibitory assay of *Hs*PGM vs ISFP1. Preincubation of ISFP1 with *Hs*PGM causes almost a twenty-fold increase in the inhibitor's potency, from 130 µM to 8 µM in 15 min. Relative activity is the normalised result over the uninhibited enzyme, set as 100% activity. Error bars are standard deviations with three determinations.

In contrast to time-dependent *Af*PGM assays, ISFP1 pre-incubation with *Hs*PGM causes an almost twenty-fold increase in potency from IC_{50} = 130 µM without pre-incubation to 8 µM after 15 min pre-incubation with the inhibitor (**Figure 10**). Additionally, instead of shifting the whole curve towards lower ISFP1 concentrations, as a result of ISFP1 increased potency, the steepness of curves changed. A closer investigation of the fitting model showed a five-fold increase in Hill slope value (from 0.6 to 2.9) between 15 min and 0 min pre-incubation periods. In this experiment's context, significant changes in the slope factor might indicate multiple non-specific labelling sites[107].

While ISFP1 appeared to display noticeable selectivity towards *Af*PGM_{WT} and *Af*PGM_{353*} over the *Hs*PGM in time-independent assays, it significantly diminished in time-dependent experiments. The changes in Hill slopes values also indicated that ISFP1 did not interact with *Hs*PGM in a drug-like manner. Additionally, attempts to perform experiments with *Hs*PGM and ISFP1 at higher concentrations of the enzyme (20 µM) and ISFP1 (200 µM) led to noticeable protein precipitation

within 3-5 min of the ISFP1 addition, further confirming that ISFP1 did not interact with human orthologue in a drug like-manner, but rather permanently deactivated the enzyme. Therefore, it is impossible to state that the ISFP1 displayed a kinetic preference toward fungal enzymes.

Reducing agents rescue inhibition of *Af*PGM$_{WT}$

ISFP1 is a relatively simple fragment composed of a thiol-reactive warhead conjugated to a hydrophobic phenyl ring decorated with fluorine and chlorine (**Figure 3**). ISFP1 covalently bound to an enzyme surface might disrupt the protein fold, causing aggregation and precipitation[96]. To exclude the possibility of precipitation-driven inhibition, a rescue experiment was designed for *Af*PGM and *Hs*PGM.

ISFP1 carries an isothiazolone warhead that forms a disulphide bond with thiols. According to a proposed mechanism of the warhead cleavage[108], the introduction of DTT would remove ISFP1 from cysteine residues by the nucleophilic attack of the mercaptothiolate (**2**) (**Figure 11A**) on the ISPF1 sulphur atom (**1**), forming an intermediate (**3**). The mercaptobutyl disulfaneyl acrylamide (**3**) would then decompose by cyclisation to form a 1,2-dithiane diol (**4**) and the thiolate (**5**). The fate of the thiolate (**5**) is dependent on the reaction conditions. Regardless of the intermediate's (**5**) fate, resulting molecules would not be able to re-form disulphide bonds in the presence of DTT in significant excess.

*Af*PGM$_{WT}$ and *Hs*PGM (5 nM) were pre-incubated with ISFP1 at 50 µM for 15 min and 0 min, followed by dithiothreitol (10 mM, 20-fold excess) at indicated time points and the addition of reaction components ($NADP^+$, *Lm*G6PDH and G1P).

As expected, labelling of *Hs*PGM with ISFP1 results in permanent enzyme deactivation that cannot be rescued by cleaving isothiazolone (**Figure 11C**). The experiment also agrees with the observed *Hs*PGM- ISFP1 IC_{50} shifts, in which time and dose-dependent fitting curves displayed an increase in the Hill slope value. Additionally, attempts to pre-incubate ISFP1 with *Hs*PGM at relatively high concentrations (enzyme concentration 20 µM, ISFP1 200 µM) caused noticeable protein precipitation.

On the other hand, the activity of *Af*PGM could be recovered (at approx. 70%) by cleaving off ISFP1 using DTT (**Figure 11B**), thus excluding precipitation as a cause for *Af*PGM inhibition. Rescuing the activity of *Af*PGM pre-incubated with the isothiazolone fragment might indicate that ISFP1 inhibits the fungal enzyme with a biological mechanism rather than promiscuous labelling resulting from its PAIN nature.

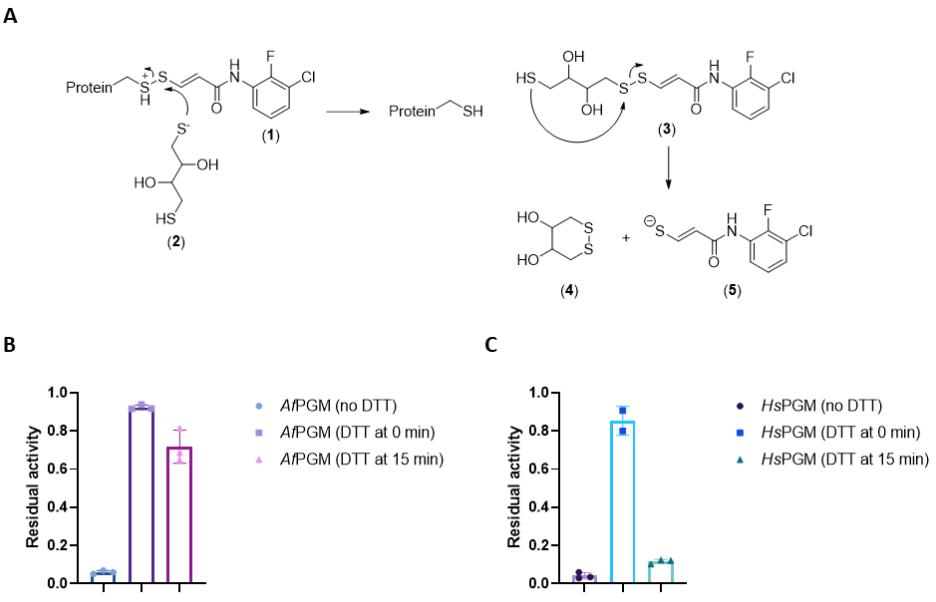

Figure 11 Activity rescue experiment; (**A**) Proposed mechanism of ISFP1 cleavage from cysteine with DTT; (**B**) DTT rescue assay for *Af*PGM$_{WT}$, after 15 min pre-incubation with ISFP1, the addition of DTT recovers approx. 70% of enzyme's activity; (**C**) DTT rescue experiment for *Hs*PGM, after 15 min pre-incubation with ISFP1, the addition of DTT rescues only 15 % of enzyme's activity. Periods in parentheses indicate the timepoint of DTT addition. Error bars are standard deviations with three determinations.

ISFP1 does not preclude binding of the substrate in *Af*PGM

Successful recombinant expression of an active *Af*PGM$_{C353V}$ showed that C353 is not required for the catalytic efficiency of *Af*PGM. Previous experiments also indicated that ISFP1 inhibited *Af*PGM, engaging cysteine 353 and did not precipitate the enzyme. The question remained, how did ISFP1 inhibit *Af*PGM?

The inhibitor-induced changes in the interaction between an enzyme and its natural substrate can be utilised to ascertain how the inhibition is elicited[109]. The Michaelis-Menten constant (K_m) provides a numerical value of substrate concentration equal to the enzyme's half-maximal velocity[110], and the turnover rate (k_{cat}) describes the maximum rate of substrate conversion[111]. Inhibitors induced dose-dependent changes in K_m and k_{cat} are often used to determine the mechanism of action. Experiments are usually performed at variable concentrations of the inhibitor and substrate (from 0.25 K_m to 5 K_m)[112]. The results can be fit to non-linear models predicting types of inhibition: competitive, non-competitive, uncompetitive or mixed[113], avoiding generating numerous plots.

Five time-independent inhibitory assays were performed to assess changes in K_m and k_{cat} as a result of *Af*PGM$_{WT}$ interaction with ISFP1. Only minor modifications were introduced. Each experiment had fixed substrate concentrations of glucose-1-phosphate at 14, 28, 56, 112 and 224 µM, and the enzyme concentration was reduced to 2 nM to slow the substrate conversion and limit it to below 10% within the read-out window. The concentration of ISFP1 was also reduced to approximately 10 times IC_{50} (20 µM to 0.312 µM in two-fold dilutions). Fluorescence results were calibrated using the calibration curve (**Figure 6**) plotted as a velocity of NADPH production against the glucose-1-phosphate concentration (**Figure 12**). Data were fitted to a local Michaelis-Menten equation (each curve was fit individually) without constricting the model of inhibition, giving basic biochemical parameters (**Table 2**) with respect to ISFP1 concentration.

The experiment provided a surprising insight into the interaction between ISFP1 and *Af*PGM. The value of K_m is relatively constant, at approx. 15 µM (**Table 2**), and does not change significantly with increments of ISFP1 concentration. On the other hand, the turnover rate, k_{cat} is decreased ten-fold by the highest concentration of ISFP from 90.5 s^{-1} to 9.1 s^{-1} (**Table 2**)

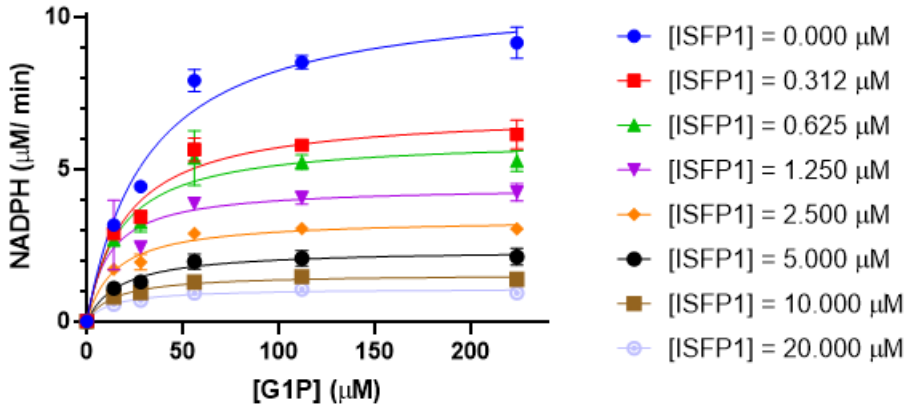

Figure 12 Plotted velocities of NADPH production against G1P concentration at different ISFP1 concentrations. Error bars are standard deviations with three determinations.

The ability of ISFP1 to decrease the *Af*PGM turnover rate in a dose-dependent manner without changing the K_m value might be explained by assuming the Michaelis-Menten constant as a substrate affinity parameter. Decreased value of k_{cat} suggests that ISFP1 induces a conformational change in *Af*PGM that slows the substrate conversion. However, a relatively constant K_m indicates that the modification of C353 does not preclude the binding of glucose-1-phosphate.

Table 2 Results of the unconstricted local fitting of *Af*PGM's velocity against glucose-1-phosphate at different ISFP1 concentrations. K_m Michaelis-Menten constant; k_{cat} turnover rate

ISFP1 (μM)	K_m (μM)	k_{cat} (s^{-1})	k_{cat}/K_m ($s^{-1}\mu M^{-1}$)
0.00	31.7 ± 7.5	90.5 ± 6.7	2.9
0.31	20.8 ± 5.5	57.5 ± 4.0	2.8
0.63	17.2 ± 6.7	50.1 ± 4.8	2.9
1.25	11.8 ± 6.7	36.9 ± 4.3	3.1
2.50	14.8 ± 3.8	28.1 ± 1.7	1.9
5.00	17.5 ± 5.9	19.7 ± 1.6	1.1
10.00	14.3 ± 5.1	13.0 ± 1.0	0.91
20.00	13.1 ± 5.7	9.1 ± 0.9	0.69

A non-isothiazolone molecule covalently inhibits *Af*PGM$_{C353*}$, but not *Af*PGM$_{C353V}$

Although ISFP1 is a covalent inhibitor[99], it is also a PAINs compound[98]. ISFP1 may interact with *Af*PGM in other non-desirable modes. Thus a different mechanism of cysteine modification is required to assess *Af*PGM's suitability for covalent inhibition. It is challenging to design a structurally similar and mild covalent inhibitor that would target *Af*PGM C353 without starting from promising hit compounds[114]. However, for proof of concept, the warhead does not need to be mild. It must modify *Af*PGM exclusively via cysteine 353 and not be an isothiazolone. Maleimides are another group of reactive warheads targeting cysteine and lysine residues[115], however, they are almost exclusive to thiols at pH 7.5 or below[116]. In contrast to isothiazolones, maleimides do not form disulphide bonds but modify cysteines in Micheal-type addition[117]. A maleimide, structurally similar (**Figure 13**) to ISFP1, was commercially available and purchased.

NPM was assessed against *Af*PGM$_{C353*}$ in both time-independent and time-dependent inhibitory assays, similarly to previous ISFP1 experiments. The pre-incubation time on this occasion was increased to 30 min, as the NPM displayed very weak potency towards *Af*PGM$_{C353*}$ without the pre-incubation time, and both *Af*PGM$_{C353*}$ and *Af*PGM$_{C353V}$ were stable at room temperature for up to 30 min.

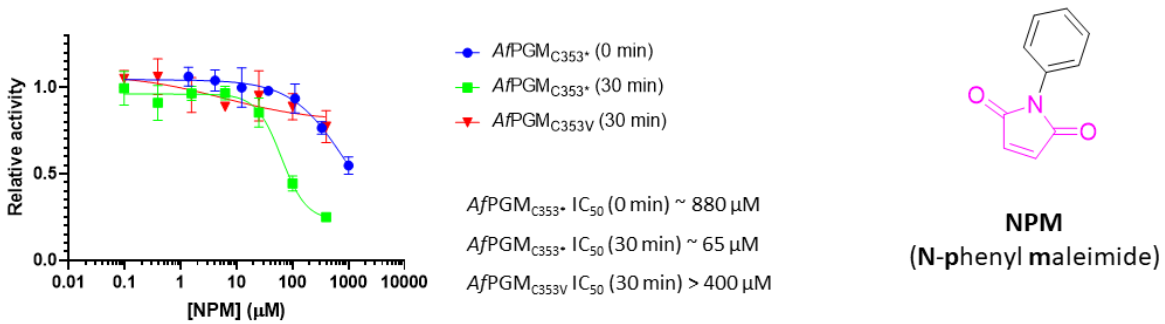

Figure 13 Time-independent and time-dependent inhibition of *Af*PGM$_{C353*}$ and *Af*PGM$_{C353V}$ and N-phenyl maleimide chemical structure. The maleimide warhead is highlighted in violet. Without pre-incubation with *Af*PGM$_{C353*}$, NPM displays weak potency toward the enzyme (extrapolated IC_{50} 880 µM); pre-incubation of NPM with *Af*PGM$_{C353*}$ for 30 min results in a twelve-fold increase in potency (IC_{50} ~65 µM); pre-incubation of *Af*PGM$_{C353V}$ with NPM for 30 min did not elicit significant inhibition of the enzyme. Relative activity is the normalised result over the uninhibited enzyme, set as 100% activity. Error bars are standard deviations with three determinations.

In the time-independent inhibitory assay, without pre-incubation of *Af*PGM$_{C353*}$ with NPM, maleimide displayed very weak potency towards the protein, with IC_{50} at approximately 880 µM (**Figure 13**, blue circles). However, pre-incubation of the molecule with the enzyme for 30 min

increased its potency twelve-fold resulting in IC_{50} at 65 µM (**Figure 13,** green squares). The lack of complete inhibition of *Af*PGM_{353*} was not a concern. NPM is not an optimised lead compound but a probe to ascertain if *Af*PGM can be exclusively inhibited via cysteine 353. To determine whether C353 is an exclusive target for N-phenyl maleimide-induced inhibition, *Af*PGM_{C353V} was pre-incubated with NPM at variable concentrations (400 µM to 0.09 µM, four-fold dilutions) for 30 min and then run in the enzymatic assay.

Surprisingly, *Af*PGM_{C353V} was not inhibited by NPM if pre-incubated with the molecule for 30 mins. The maleimide displays very weak enzyme impairment at 400 µM of NPM (**Figure 13,** red triangles), indicating that covalent inhibition in *Af*PGM was exclusively elicited via cysteine 353. Although enzyme assays showed the lack of *Af*PGM_{C353V} inhibition with NPM, they did not provide insight into an enzyme labelling stoichiometry.

To confirm the NPM labelling stoichiometry of *Af*PGM_{C353*} and assess the modification of *Af*PGM_{C353V}, both muteins were tested by intact mass spectrometry. Enzymes (200 µL, 20µM) were pre-incubated with NPM (400 µM) for 30 mins in MOPS (50 mM, pH=7.4), then dialysed to a fresh buffer (200 mL) for 8 h at 4^{o}C and analysed by LC-MS. The theoretical masses of enzymes were calculated in Expasy.

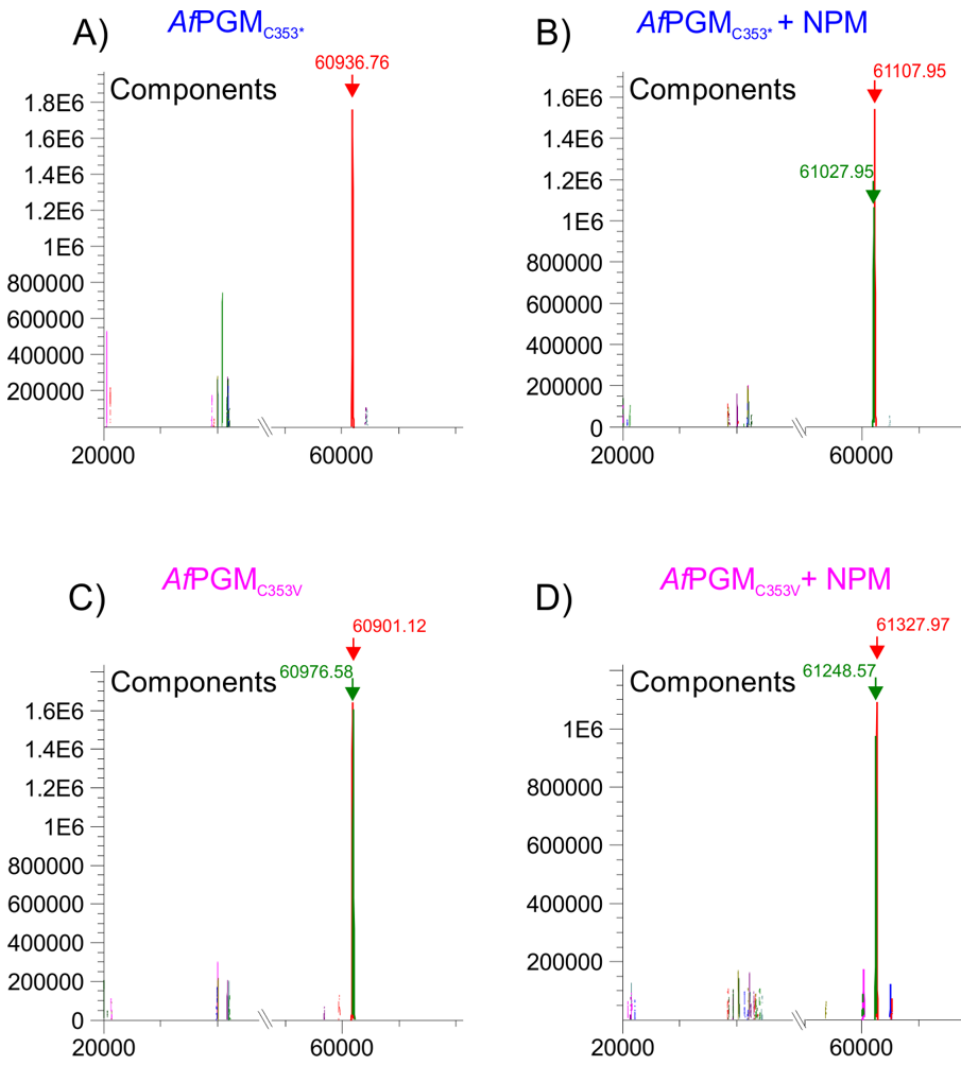

Figure 14 Intact mass spectrometry results of *Af*PGM$_{C353}$* and *Af*PGM$_{C353V}$ pre-incubated with NPM (400 µM) for 30 min. **Panel A** The theoretical molecular weight of unmodified *Af*PGM$_{C353*}$ is 60864.76 Da, while the MS spectrum found 60936.76 Da, which corresponds to a mass of phosphorylated *Af*PGM$_{C353*}$ (72-80 Da, phosphonate adduct). **Panel B** The spectrum of NPM-modified *Af*PGMC$_{353*}$ gave two major peaks with similar masses, 61107.95 Da (**red**) corresponding to phosphorylated *Af*PGM$_{C353*}$ and labelled by molecule with Mw of 171.19 Da, which is consistent with the mass of NPM (173.17 Da) and the second peak 61027.95 Da (**green**) displays the molecular weight of dephosphorylated AfPGM$_{C353*}$ modified by single NPM molecule. **Panel C** Theoretical mass of unmodified *Af*PGM$_{C353V}$ is 60908.94 Da. The mass spectrometry found 60901.76 Da (**red**) and 60976.58 (**green**), consistent with dephosphorylated and phosphorylated *Af*PGM$_{C353}$. **Panel D** The pre-incubation of NPM with *Af*PGM$_{C353V}$ yielded two species, 61248.57 (**green**) corresponding to dephosphorylated protein modified by adduct with a mass of 346.31 Da, in agreement with a mass of two NPM molecules, and 61327.97 (**red**) phosphorylated *Af*PGM$_{C353V}$ also labelled by two molecules of NPM.

Unsurprisingly, *Af*PGM$_{C353*}$ displays a single modification, with a mass shift of 171 Da corresponding to the mass of NPM (173.15 Da) (**Figure 14** Panel **B**) (**Table 3**). The absence of noticeable protein species with multiple NPM modifications indicates that N-phenyl maleimide labels only thiols under

these experimental conditions. Despite the lack of *Af*PGM$_{C353V}$ inhibition by NPM, the intact mass spectrometry indicates the labelling of two thiols (**Figure 14** Panel **D**) (**Table 3**), most likely C131 and C242, both solvent exposed. Both inhibitory assays and intact mass spectrometry strongly indicated that NPM acted via cysteine C353 to elicit the enzyme inhibition. Adduct formation with other cysteines, either C131, C242 or C364, is not enough to impair *Af*PGM's activity.

Table 3 Intact mass spectrometry results of *Af*PGM$_{C353*}$ and *Af*PGM$_{C353V}$ against NPM. Da mass in Daltons, PO_3^{2-} phosphonate with the mass of 80 Da

enzyme (unmodified)	**Theoretical mass (Da)**	**MS found (Da)**
*Af*PGM$_{C353*}$ + PO_3^{2-}	60943.732	60936.76
*Af*PGM$_{C353V}$	60908.94	60901.12
*Af*PGM$_{C353V}$ + PO_3^{2-}	60988.94	60976.58
Enzyme (NPM modified)	**Theoretical mass (Da)**	**MS found (Da)**
*Af*PGM$_{C353*}$ (single modification)	61037.760	61027.95
*Af*PGM$_{C353*}$ + PO_3^{2-} (single modification)	61116.732	61107.95
*Af*PGM$_{C353V}$ (double modification)	61255.24	61248.57
*Af*PGM$_{C353V}$ + PO_3^{2-} (double modification)	61335.24	61327.97

NPM occupancy on *Af*PGM$_{C353*}$ can be detected in the plate-based assay

Genetic studies suggested that *Af*PGM is an essential enzyme[70]. Thus, it might constitute a potential target for novel antifungals. However, it still lacks an acceptable chemical probe that could be used to attempt to phenocopy a genetic phenotype *in cellulo.* Although ISFP1 and NPM were successfully used as inhibitors in the recombinant assays, they are unsuitable for cellular assays due to their reactivity and promiscuity[96,117]. A new mild and selective covalent modifier is required to exploit the non-conserved C353 in *A. fumigatus*. A rational design of such an inhibitor would be very challenging due to the lack of crystallographic data on *Af*PGM with ISFP1. Therefore a screen with covalent fragments could potentially yield a promising non-PAINs chemical entity. Although the inhibitory assays were optimised for high-throughput inhibitory screens, the example of NPM showed that fragments might elicit only partial inhibition, despite forming an adduct with cysteine C353. Additionally, inhibitory assays require a coupling enzyme which further complicates kinetic equations by introducing 6-phosphogluconolactone, a by-product of $NADP^+$ reduction, which can potentially inhibit both PGM as well as G6PDH.

Success with N-phenyl maleimide sparked an idea for designing an occupancy assay using different maleimide- 7-diethylamino-3-(4'-maleimidylphenyl)-4-methylcoumarin also known as CPM[118]. CPM is a fluorophore with a maleimide warhead, frequently used to quantify free thiols in various assays. The maleimide warhead in CPM is both a thiol labelling agent and a fluorescence quencher. Maleimide is a powerful electron-withdrawing moiety, which significantly reduces the fluorescence of the methyl coumarin (the fluorophore), eliciting the so-called "inner filter effect"[119]. Once the maleimide binds the thiol, the withdrawing effects are reduced, and the coumarin can emit light[120] Theoretically, *Af*PGM$_{353*}$ can be treated as a free thiol, and if sterically possible, CPM could react with cysteine C353 if not occupied by NPM (**Figure 15**).

To assess the usefulness of CPM in designing an occupancy assay, *Af*PGM$_{C353*}$ (20 µM) was pre-incubated with NPM (at various concentrations) for 60 min at room temperature, then diluted 100-fold and added to solutions of CPM (20 µM). The baseline serving in this assay contained appropriately diluted NMP with CPM (20 µM) and without the enzyme.

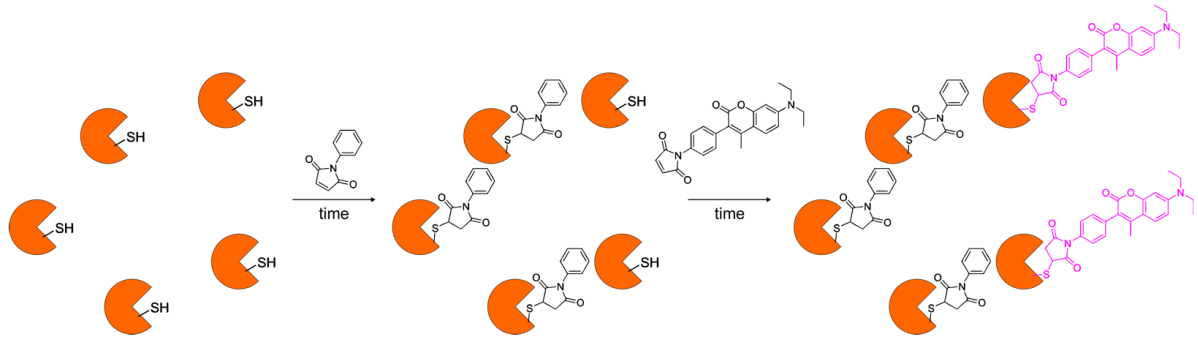

Figure 15 Premise of the CPM assay. A macromolecule is first allowed to react with NPM. Adducts are formed based on the NPM's potency towards the protein. After the pre-incubation period, CPM is added, and it will form an adduct with all cysteines that NPM does not occupy. Violet CPM represents the fluorescent form of 7-diethylamino-3-(4'-maleimidylphenyl)-4-methylcoumarin, while black represents the form of non-fluorescent CPM.

The experimental design was limited by the highest possible concentration of CPM in aqueous solutions (approx. 20 μM). The assay was conducted in so-called jump dilution to avoid competition between CPM and NPM for C353. The preincubation between ligand and protein was performed at high concentrations of both participants, then diluted to a solution of CPM in a buffer.

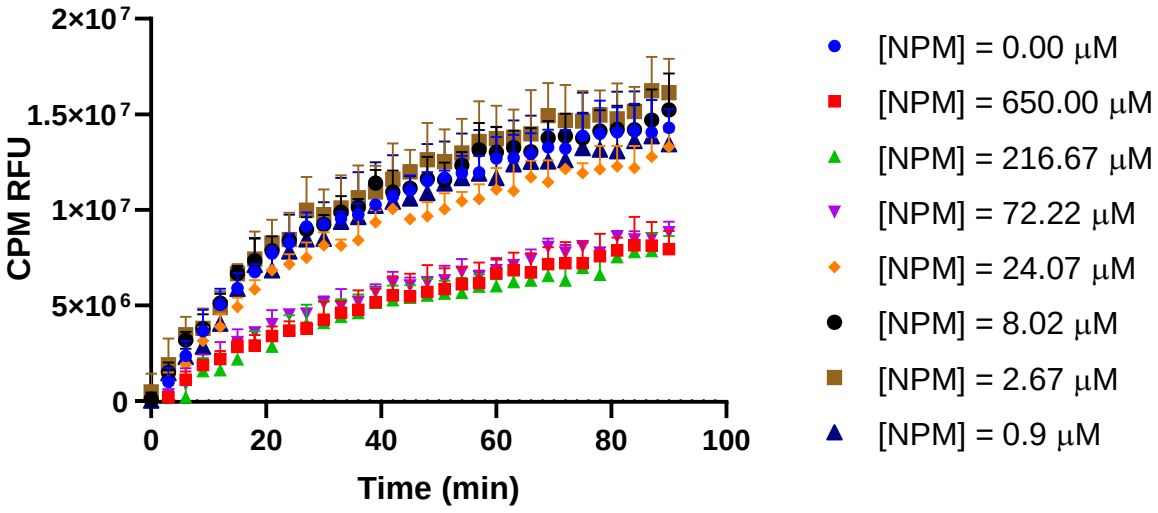

Figure 16 CPM assay of NPM vs *Af*PGM$_{C353*}$; *Af*PGM$_{C353*}$ (20 μM) was pre-incubated with NPM (at various concentrations) for 60 min at room temperature, then diluted 100-times and added to solutions of CPM (20 μM). The baseline serving in this assay contained NMP at 6.50, 2.16, 0.72, 0.24, 0.08, 0.03 and 0.0009 μM, with CPM (20 μM) and without the enzyme. *Af*PGM$_{353*}$ pre-incubated with NPM at 650 μM, 216 μM and 72 μM displayed visibly lower CPM fluorescence than the unmodified enzyme. Error bars are standard deviations with three determinations.

Pre-incubation of *Af*PGM$_{C353*}$ with NPM, in a ratio of at least 3:1, showed a noticeable difference in CPM fluorescence (**Figure 13,** black circles, brown square and dark blue triangles) in comparison to the unmodified enzyme (**Figure 13,** Blue circles) indicating cysteine labelling by N-phenyl maleimide. With lower ratios of protein and the inhibitor (at or below 20 µM), there was no observable labelling of C353. Two factors may play a significant role. The NPM dose-independent increase in fluorescence may indicate non-thiol CPM binding, hiding the reduced signal from protein samples pre-incubated with CPM at ratios of 1:1 or lower. On the other hand, speculatively, the NPM adduct formation might not be driven entirely by the reactivity of maleimide. The concentration of NPM might be below the K_i (inhibitory constant) required to form an initial non-covalent binary complex, especially considering that the assay was designed in a depletion regime.

Although the data quality is poor, NPM occupancy can be detected, opening a possibility to optimise the assay. There are numerous maleimide-based fluorophores utilised in thiol quantification[121,122]. They may offer better signal-to-background ratio, faster kinetics or better aqueous solubility.

Discussion

Aspergillus fumigatus infections are persistent, difficult to treat and have a poor recovery prognosis[31]. Current therapies are failing[123], and no new drugs are on the horizon. The major problem with finding novel medicines and drug targets is the lack of chemically and genetically validated enzymes[124]. The gene encoding phosphoglucomutase in *Aspergillus fumigatus* stands out as an essential and potentially druggable enzyme. However, whether the enzyme's importance comes from its enzymatic or non-enzymatic function is still unknown. Chemical phenocopy of lethality seen in a PGM knockdown would further validate *Af*PGM as a viable target for developing novel antifungals.

A fragment screening campaign found a small thiol-reactive molecule to inhibit recombinantly expressed *Af*PGM. Unfortunately, the hit fragment was an isothiazolone-based molecule, widely considered a covalent pan-interference compound (PAIN)[96–98]. Although PAINS compounds are seen as a waste of time and money[125], this work aimed to exploit both isothiazolone and maleimide to probe *Af*PGM and gain insight into the possibility of developing non-PAINs covalent inhibitors.

Experiments utilising both control muteins *Af*PGM$_{C353*}$ and *Af*PGM$_{C353V}$ showed that *Af*PGM is inhibited by ISFP1 through cysteine C353, a residue that is not conserved in human PGM. However, the hit fragment did not exhibit selectivity towards the fungal orthologue over the human enzyme. The scientific community is understandably sceptical towards isothiazolones[96,97,125,126]. They might interact with their protein targets in an unwanted manner. N-phenyl maleimide was used to ascertain whether warheads other than isothiazolones could inhibit *Af*PGM by modifying C353. Although maleimides are also thiol-reactive molecules[117], they utilise a different chemical mechanism of cysteine modification. A maleimide structurally similar to ISFP1 inhibited *Af*PGM$_{C353*}$ but did not inhibit *Af*PGM$_{C353V}$, which corroborates with the data obtained from ISFP1 experiments. All results conclude that *AfP*GM is a promising candidate for covalent inhibition. Despite the success of isothiazolones and maleimides in recombinant protein assays, their use in cellular assays would not produce valid results. Both warhead types are too promiscuous and reactive and most likely would form adducts with off-targets in *A. fumigatus*[100,117]. Therefore a new chemical entity is required. A simple plate-based CPM assay was designed to open the possibility of a covalent screen. Although preliminary experiments showed that covalent adduct could be detected, the data quality was poor, most likely resulting from CPM labelling lysine residues. The assay could be optimised for semi-high-throughput screens, allowing accessible assessment of emerging covalent fragments/molecule libraries[127]. Fortunately, CPM is not the only fluorophore used in thiol labelling assays. ThioGlo™, a

series of different maleimide-based fluorophores, might provide a better signal-to-background ratio, faster labelling kinetics or higher selectivity towards cysteine residues [121,122].

This work has unveiled, beyond doubt, that cysteine C353, a non-conserved residue, can be exploited for covalent inhibition, either by isothiazolone or maleimide. However, how the labelling of cysteine C353 in *Af*PGM leads to inhibition is not yet clear. Experiments performed at variable substrate concentrations in the presence of ISFP1 indicated that the inhibitor might preclude conformational changes in *Af*PGM. The kinetic parameters of inhibited *Af*PGM showed a relatively constant value of K_m (approx. 15 µM) and the dose-dependent decrements of k_{cat}, reaching a value 10-fold lower than the uninhibited enzyme. In parts, the Michaelis-Menten (K_m) constant can be viewed as a substrate affinity constant[110]. Therefore, it is plausible that ISFP1 binding does not influence substrate recognition, which agrees with the ISFP1 dose-dependent constant value of K_m. On the other hand, the ISFP1 dose-dependent decreasing value of k_{cat} may indicate slowing the substrate conversion. *Af*PGM, similarly to other α-D-phosphohexomutase, adopts at least two known conformations, opened, a closed, and both are the consequence of domain IV motion[89]. Some evidence suggests that domains I-III also change their conformation to stabilise the transition state of the phosphoryl transfer[70]. A pocket containing cysteine 353 is located at the interface of domains I-III (**Figure 2B**). Insertion of a small molecule that is large enough to introduce steric hindrance may preclude the motion of domains. Thus, adopting closed conformation, required for the phosphate transfer, would be altered. The definitive proof could come from structural data on *Af*PGM and ISFP1. Unfortunately, every attempt to co-crystalise *Af*PGM with ISFP1 was unsuccessful[70]. The closest structural data on the interaction between ISFP1 and PGM can be extracted from the co-crystal structure of *Ca*PGM and ISFP1. However, no significant differences were observed between the crystal structures of *Ca*PGM and co-crystal structure of *Ca*PGM and ISFP1 except the tryptophan 355 motion (W349 in *Af*PGM). In a *Ca*PGM-ISFP1 co-crystal structure, W355 flipped out to the protein surface, opening the cryptic pocket containing C359, the location of ISFP1 adduct. Perhaps, a large and hydrophobic residue on the protein surface between domains I-III precludes their motion resulting in an impairment of *Ca*PGM enzymatic activity. A similar mechanism might be present in *Af*PGM. The ISFP1-induced pocket is almost identical in *Af*PGM and *Ca*PGM.

In summary, PAINs compounds can be helpful if treated with caution. Questions asked at the beginning of this project have been answered. Inhibition of *Af*PGM occurs via cysteine C353 and control muteins *Af*PGM$_{353*}$, and *Af*PGMC$_{353V}$ confirmed this with both isothiazolone and maleimide warheads. Successful rescue of ISFP1 pre-incubation with *Af*PGM also indicated that inhibition is not a result of protein precipitation. A similar experiment could not be done for NPM, a maleimide fragment. Although the so-called retro-Michael addition (opening of the maleimide ring) happens in

nature[128], it does not cause adduct removal from the cysteine residue[129]. Complete removal of maleimide would probably require conditions also denaturing enzymes.

The mechanism of *Af*PGM inhibition was not wholly unveiled. However, I hypothesise that the modification of cysteine C353 by ISFP1 interferes with the motion of key domains, disrupting a sequence of conformational changes that are required for successful phosphoryl transfer.

Although the concept of *Af*PGM inhibition via C353, a non-conserved cysteine in human orthologue, was established, the chemical probes used in the project are unsuitable for further development. It is still unknown if a mild covalent inhibitor would impair the activity of *Af*PGM, which raises the question if *Af*PGM is a potentially novel and druggable antifungal target. The lack of crystallographic data on *Af*PGM with ISFP1 limits the possibility of a rational inhibitor design. Perhaps attempting to obtain the co-crystal structure of *Af*PGMC_{353*} with NPM could provide some structural insight into the mechanism of inhibition. However, in the context of drug discovery, NPM is still a PAINs compound, arguably more potent than isothiazolone derivatives, thus the hypothetical co-crystal structure of *Af*PGM$_{C353*}$ may provide only artifactual information. As an alternative to rational design, screens could be performed. A covalent screen would be an obvious choice, either by mass spectrometry or by further developing fluorescence-based assays using commercial drug-like small molecules or fragment libraries. However, the selection of libraries must be careful to avoid any potential PAINs hits. The non-covalent screen would be a less obvious choice. Finding a non-covalent scaffold that could be further developed into a covalent inhibitor is possible. However, it is more challenging than growing or expanding hypothetical covalent hit. It is also worth pointing out that several non-covalent analogues of ISFP1 where isothiazolone ring was substituted to either imidazoles, triazoles, and thiazoles conjugated to a phenyl ring with different decorations did not inhibit recombinantly expressed *Af*PGM$_{WT}$. It would probably be better not to limit non-covalent screens to ISFP1 or NPM-like molecules but to find a new scaffold.

References

(1) Latgé, J. P. Aspergillus Fumigatus and Aspergillosis. *Clin. Microbiol. Rev.* **1999**, *12* (2), 310–350. https://doi.org/10.1128/cmr.12.2.310.

(2) Kwon-Chung, K. J.; Sugui, J. A. Aspergillus Fumigatus-What Makes the Species a Ubiquitous Human Fungal Pathogen? *PLoS Pathog.* **2013**, *9* (12), 1–4. https://doi.org/10.1371/journal.ppat.1003743.

(3) Smith, N. L.; Denning, D. W. Underlying Conditions in Chronic Pulmonary Aspergillosis Including Simple Aspergilloma. *Eur. Respir. J.* **2011**, *37* (4), 865–872. https://doi.org/10.1183/09031936.00054810.

(4) Muthu, V.; Rudramurthy, S. M.; Chakrabarti, A.; Agarwal, R. Epidemiology and Pathophysiology of COVID-19-Associated Mucormycosis: India Versus the Rest of the World. *Mycopathologia* **2021**, *186* (6), 739–754. https://doi.org/10.1007/s11046-021-00584-8.

(5) Saral, R. Candida and Aspergillus Infections in Immunocompromised Patients: An Overview. *Rev. Infect. Dis.* **1991**, *13* (3), 487–492. https://doi.org/10.1093/clinids/13.3.487.

(6) Moran, C.; Grussemeyer, C. A.; Spalding, J. R.; Benjamin, D. K.; Reed, S. D. Candida Albicans and Non-Albicans Bloodstream Infections in Adult and Pediatric Patients: Comparison of Mortality and Costs. *Pediatr. Infect. Dis. J.* **2009**, *28* (5), 433–435. https://doi.org/10.1097/INF.0b013e3181920ffd.

(7) Kanj, A.; Abdallah, N.; Soubani, A. O. The Spectrum of Pulmonary Aspergillosis. *Respir. Med.* **2018**, *141* (March), 121–131. https://doi.org/10.1016/j.rmed.2018.06.029.

(8) Sun, K. S.; Tsai, C. F.; Chen, S. C. C.; Huang, W. C. Clinical Outcome and Prognostic Factors Associated with Invasive Pulmonary Aspergillosis: An 11-Year Follow-up Report from Taiwan. *PLoS One* **2017**, *12* (10), 1–10. https://doi.org/10.1371/journal.pone.0186422.

(9) Reichenberger, F.; Habicht, J. M.; Gratwohl, A.; Tamm, M. Diagnosis and Treatment of Invasive Pulmonary Aspergillosis in Neutropenic Patients. *Eur. Respir. J.* **2002**, *19* (4), 743–755. https://doi.org/10.1183/09031936.02.00256102.

(10) Maertens, J. A. History of the Development of Azole Derivatives. *Clin. Microbiol. Infect.* **2004**, *10* (SUPPL. 1), 1–10. https://doi.org/10.1111/j.1470-9465.2004.00841.x.

(11) Cappelletty, D.; Eiselstein-McKitrick, K. The Echinocandins. *Pharmacotherapy* **2007**, *27* (3), 369–388. https://doi.org/10.1592/phco.27.3.369.

(12) Carolus, H.; Pierson, S.; Lagrou, K.; Van Dijck, P. Amphotericin b and Other Polyenes—Discovery, Clinical Use, Mode of Action and Drug Resistance. *J. Fungi* **2020**, *6* (4), 1–20. https://doi.org/10.3390/jof6040321.

(13) Cavassin, F. B.; Baú-Carneiro, J. L.; Vilas-Boas, R. R.; Queiroz-Telles, F. Sixty Years of Amphotericin B: An Overview of the Main Antifungal Agent Used to Treat Invasive Fungal Infections. *Infect. Dis. Ther.* **2021**, *10* (1), 115–147. https://doi.org/10.1007/s40121-020-00382-7.

(14) Rodrigues, M. L. The Multifunctional Fungal Ergosterol. *mBio*. 2018, pp 1–5. https://doi.org/10.1128/mBio.01755-18.

(15) Campoy, S.; Adrio, J. L. Antifungals. *Biochem. Pharmacol.* **2017**, *133*, 86–96. https://doi.org/10.1016/j.bcp.2016.11.019.

(16) Dotis, J.; Simitsopoulou, M.; Dalakiouridou, M.; Konstantinou, T.; Panteliadis, C.; Walsh, T. J.; Roilides, E. Amphotericin B Formulations Variably Enhance Antifungal Activity of Human Neutrophils and Monocytes against Fusarium Solani: Comparison with Aspergillus Fumigatus. *J. Antimicrob. Chemother.* **2008**, *61* (4), 810–817. https://doi.org/10.1093/jac/dkn036.

(17) Allen, D.; Wilson, D.; Drew, R.; Perfect, J. Azole Antifungals: 35 Years of Invasive Fungal Infection Management. *Expert Rev. Anti. Infect. Ther.* **2015**, *13* (6), 787–798. https://doi.org/10.1586/14787210.2015.1032939.

(18) Wall, G.; Lopez-Ribot, J. L. Current Antimycotics, New Prospects, and Future Approaches to Antifungal Therapy. *Antibiotics* **2020**, *9* (8), 1–10. https://doi.org/10.3390/antibiotics9080445.

(19) Gintjee, T. J.; Donnelley, M. A.; Thompson, G. R. Aspiring Antifungals: Review of Current Antifungal Pipeline Developments. *J. Fungi* **2020**, *6* (1), 28. https://doi.org/10.3390/jof6010028.

(20) Shrestha, S. K.; Garzan, A.; Garneau-Tsodikova, S. Novel Alkylated Azoles as Potent Antifungals. *Eur. J. Med. Chem.* **2017**, *133*, 309–318. https://doi.org/10.1016/j.ejmech.2017.03.075.

(21) Sobel, J. D.; Nyirjesy, P. Oteseconazole: An Advance in Treatment of Recurrent Vulvovaginal Candidiasis. *Future Microbiol.* **2021**, *16* (18), 1453–1461. https://doi.org/10.2217/fmb-2021-0173.

(22) Perfect, J. R. The Antifungal Pipeline: A Reality Check. *Nat. Rev. Drug Discov.* **2017**, *16* (9), 603–616. https://doi.org/10.1038/nrd.2017.46.

(23) Berger, S.; Chazli, Y. El; Babu, A. F.; Coste, A. T. Azole Resistance in Aspergillus Fumigatus: A Consequence of Antifungal Use in Agriculture? *Front. Microbiol.* **2017**, *8* (JUN), 1–6. https://doi.org/10.3389/fmicb.2017.01024.

(24) Rybak, J. M.; Fortwendel, J. R.; Rogers, P. D. Emerging Threat of Triazole-Resistant Aspergillus Fumigatus. *J. Antimicrob. Chemother.* **2019**, *74* (4), 835–842. https://doi.org/10.1093/jac/dky517.

(25) Guegan, H.; Prat, E.; Robert-Gangneux, F.; Gangneux, J. P. Azole Resistance in Aspergillus Fumigatus: A Five-Year Follow Up Experience in a Tertiary Hospital With a Special Focus on Cystic Fibrosis. *Front. Cell. Infect. Microbiol.* **2021**, *10* (February), 1–9. https://doi.org/10.3389/fcimb.2020.613774.

(26) Aruanno, M.; Glampedakis, E.; Lamoth, F. Echinocandins for the Treatment of Invasive Aspergillosis: From Laboratory to Bedside. *Antimicrob. Agents Chemother.* **2019**, *63* (8). https://doi.org/10.1128/AAC.00399-19.

(27) McCarty, T. P.; Pappas, P. G. Antifungal Pipeline. *Front. Cell. Infect. Microbiol.* **2021**, *11* (September), 1–11. https://doi.org/10.3389/fcimb.2021.732223.

(28) Lee, A. Ibrexafungerp: First Approval. *Drugs* **2021**, *81* (12), 1445–1450. https://doi.org/10.1007/s40265-021-01571-5.

(29) Jallow, S.; Govender, N. P. Ibrexafungerp: A First-in-Class Oral Triterpenoid Glucan Synthase Inhibitor. *J. Fungi* **2021**, *7* (3), 1–19. https://doi.org/10.3390/jof7030163.

(30) Colombo, R. E.; Vazquez, J. A. An Evaluation of Ibrexafungerp for the Treatment of Invasive Candidiasis: The Evidence to Date. *Expert Opin. Pharmacother.* **2021**, *22* (7), 797–807. https://doi.org/10.1080/14656566.2021.1890026.

(31) Lowes, D.; Al-Shair, K.; Newton, P. J.; Morris, J.; Harris, C.; Rautemaa-Richardson, R.; Denning, D. W. Predictors of Mortality in Chronic Pulmonary Aspergillosis. *Eur. Respir. J.* **2017**, *49* (2), 1–10. https://doi.org/10.1183/13993003.01062-2016.

(32) Latgé, J. P.; Chamilos, G. Aspergillus Fumigatus and Aspergillosis in 2019. *Clin. Microbiol. Rev.* **2020**, *33* (1). https://doi.org/10.1128/CMR.00140-18.

(33) Firacative, C. Invasive Fungal Disease in Humans: Are We Aware of the Real Impact? *Mem. Inst. Oswaldo Cruz* **2020**, *115* (9), 1–9. https://doi.org/10.1590/0074-02760200430.

(34) Liu, L.; Gu, Y.; Wang, Y.; Shen, K.; Su, X. The Clinical Characteristics of Patients With Nonneutropenic Invasive Pulmonary Aspergillosis. *Front. Med.* **2021**, *8* (February). https://doi.org/10.3389/fmed.2021.631461.

(35) Bongomin, F.; Gago, S.; Oladele, R. O.; Denning, D. W. Global and Multi-National Prevalence of Fungal Diseases—Estimate Precision. *J. Fungi* **2017**, *3* (4). https://doi.org/10.3390/jof3040057.

(36) Trof, R. J.; Beishuizen, A.; Debets-Ossenkopp, Y. J.; Girbes, A. R. J.; Groeneveld, A. B. J. Management of Invasive Pulmonary Aspergillosis in Non-Neutropenic Critically Ill Patients. *Intensive Care Med.* **2007**, *33* (10), 1694–1703. https://doi.org/10.1007/s00134-007-0791-z.

(37) Rauseo, A. M.; Coler-Reilly, A.; Larson, L.; Spec, A. Hope on the Horizon: Novel Fungal Treatments in Development. *Open Forum Infect. Dis.* **2020**, *7* (2), 1–19. https://doi.org/10.1093/ofid/ofaa016.

(38) Pré, S.; Beckmann, N.; Almeida, C.; Sibley, G. E. M.; Law, D.; Brand, A. C.; Birch, M.; Read, N. D.; Oliver, D. Effect of the Novel Antifungal Drug F901318 (Olorofim) on Growth and Viability of Aspergillus Fumigatus. **2018**, *901318*, 1–11.

(39) Zhen, C.; Lu, H.; Jiang, Y. Novel Promising Antifungal Target Proteins for Conquering Invasive Fungal Infections. *Front. Microbiol.* **2022**, *13* (June). https://doi.org/10.3389/fmicb.2022.911322.

(40) Shaw, K. J.; Ibrahim, A. S. Fosmanogepix: A Review of the First-in-Class Broad Spectrum Agent for the Treatment of Invasive Fungal Infections. *J. Fungi* **2020**, *6* (4), 1–21. https://doi.org/10.3390/jof6040239.

(41) Pfaller, M. A.; Huband, M. D.; Flamm, R. K.; Bien, P. A.; Castanheira, M. Antimicrobial Activity of Manogepix, a First-in-Class Antifungal, and Comparator Agents Tested against Contemporary Invasive Fungal Isolates from an International Surveillance Programme (2018–2019). *J. Glob. Antimicrob. Resist.* **2021**, *26*, 117–127. https://doi.org/10.1016/j.jgar.2021.04.012.

(42) Vahedi-Shahandashti, R.; Lass-Flörl, C. Novel Antifungal Agents and Their Activity against Aspergillus Species. *J. Fungi* **2020**, *6* (4), 1–21. https://doi.org/10.3390/jof6040213.

(43) Kim, Y.; Alarcon, S.; Lee, S.; Lee, M.-J.; Giaccone, G.; Neckers, L.; Trepel, J. Update on Hsp90 Inhibitors in Clinical Trial. *Curr. Top. Med. Chem.* **2009**, *9* (15), 1479–1492. https://doi.org/10.2174/156802609789895728.

(44) Fukuyo, Y.; Hunt, C. R.; Horikoshi, N. Geldanamycin and Its Anti-Cancer Activities. *Cancer Lett.* **2010**, *290* (1), 24–35. https://doi.org/10.1016/j.canlet.2009.07.010.

(45) Lamoth, F.; Juvvadi, P. R.; Gehrke, C.; Steinbacha, W. J. In Vitro Activity of Calcineurin and Heat Shock Protein 90 Inhibitors against Aspergillus Fumigatus Azole- and Echinocandin-Resistant Strains. *Antimicrob. Agents Chemother.* **2013**, *57* (2), 1035–1039. https://doi.org/10.1128/AAC.01857-12.

(46) Lamoth, F.; Juvvadi, P. R.; Steinbach, W. J. Histone Deacetylase Inhibition as an Alternative Strategy against Invasive Aspergillosis. *Front. Microbiol.* **2015**, *6* (FEB), 4–9. https://doi.org/10.3389/fmicb.2015.00096.

(47) Sun, D.; Gao, W.; Hu, H.; Zhou, S. Why 90% of Clinical Drug Development Fails and How to Improve It? *Acta Pharm. Sin. B* **2022**, *12* (7), 3049–3062. https://doi.org/10.1016/j.apsb.2022.02.002.

(48) Hurtado-Guerrero, R.; Raimi, O. G.; Min, J.; Zeng, H.; Vallius, L.; Shepherd, S.; Ibrahim, A. F. M.; Wu, H.; Plotnikov, A. N.; van Aalten, D. M. F. Structural and Kinetic Differences between Human and Aspergillus Fumigatus D-Glucosamine-6-Phosphate N-Acetyltransferase. *Biochem. J.* **2008**, *415* (2), 217–223. https://doi.org/10.1042/BJ20081000.

(49) Garcia-Rubio, R.; de Oliveira, H. C.; Rivera, J.; Trevijano-Contador, N. The Fungal Cell Wall: Candida, Cryptococcus, and Aspergillus Species. *Front. Microbiol.* **2020**, *10* (January), 1–13. https://doi.org/10.3389/fmicb.2019.02993.

(50) Gilbert, H. J. The Biochemistry and Structural Biology of Plant Cell Wall Deconstruction. *Plant Physiol.* **2010**, *153* (2), 444–455. https://doi.org/10.1104/pp.110.156646.

(51) Lima, S. L.; Colombo, A. L.; de Almeida Junior, J. N. Fungal Cell Wall: Emerging Antifungals and Drug Resistance. *Front. Microbiol.* **2019**, *10* (November), 1–9. https://doi.org/10.3389/fmicb.2019.02573.

(52) Kang, X.; Kirui, A.; Muszyński, A.; Widanage, M. C. D.; Chen, A.; Azadi, P.; Wang, P.; Mentink-Vigier, F.; Wang, T. Molecular Architecture of Fungal Cell Walls Revealed by Solid-State NMR. *Nat. Commun.* **2018**, *9* (1), 1–12. https://doi.org/10.1038/s41467-018-05199-0.

(53) Lee, M. J.; Sheppard, D. C. Recent Advances in the Understanding of the Aspergillus Fumigatus Cell Wall. *J. Microbiol.* **2016**, *54* (3), 232–242. https://doi.org/10.1007/s12275-016-6045-4.

(54) Ruiz-Herrera, J.; Ortiz-Castellanos, L. Cell Wall Glucans of Fungi. A Review. *Cell Surf.* **2019**, *5* (March), 100022. https://doi.org/10.1016/j.tcsw.2019.100022.

(55) Jenks, J. D.; Hoenigl, M. Treatment of Aspergillosis. *J. Fungi* **2018**, *4* (3), 1–17. https://doi.org/10.3390/jof4030098.

(56) Glöckner, A.; Steinbach, A.; Vehreschild, J. J.; Cornely, O. A. Treatment of Invasive Candidiasis with Echinocandins. *Mycoses* **2009**, *52* (6), 476–486. https://doi.org/10.1111/j.1439-0507.2008.01645.x.

(57) Walker, S. S.; Xu, Y.; Triantafyllou, I.; Waldman, M. F.; Mendrick, C.; Brown, N.; Mann, P.; Chau, A.; Patel, R.; Bauman, N.; Norris, C.; Antonacci, B.; Gurnani, M.; Cacciapuoti, A.; McNicholas, P. M.; Wainhaus, S.; Herr, R. J.; Kuang, R.; Aslanian, R. G.; Ting, P. C.; Black, T. A. Discovery of a Novel Class of Orally Active Antifungal β-1,3-D-Glucan Synthase Inhibitors. *Antimicrob. Agents Chemother.* **2011**, *55* (11), 5099–5106. https://doi.org/10.1128/AAC.00432-11.

(58) Petraitis, V.; Petraitiene, R.; Katragkou, A.; Maung, B. B. W.; Naing, E.; Kavaliauskas, P.; Barat, S.; Borroto-Esoda, K.; Azie, N.; Angulo, D.; Walsh, T. J. Combination Therapy with Ibrexafungerp (Formerly SCY-078), a First-in-Class Triterpenoid Inhibitor of (1-3)-β-D-Glucan Synthesis, and Isavuconazole for Treatment of Experimental Invasive Pulmonary Aspergillosis. *Antimicrob. Agents Chemother.* **2020**, *64* (6). https://doi.org/10.1128/AAC.02429-19.

(59) Lenardon, M. D.; Munro, C. A.; Gow, N. A. R. Chitin Synthesis and Fungal Pathogenesis. *Curr. Opin. Microbiol.* **2010**, *13* (4), 416–423. https://doi.org/10.1016/j.mib.2010.05.002.

(60) Rogg, L. E.; Fortwendel, J. R.; Juvvadi, P. R.; Steinbach, W. J. Regulation of Expression, Activity and Localization of Fungal Chitin Synthases. *Med. Mycol.* **2012**, *50* (1), 2–17. https://doi.org/10.3109/13693786.2011.577104.

(61) Steinbach, W. J.; Stevens, D. A. Review of Newer Antifungal and Immunomodulatory Strategies for Invasive Aspergillosis. *Clin. Infect. Dis.* **2003**, *37* (s3), S157–S187. https://doi.org/10.1086/376523.

(62) Henry, C.; Fontaine, T.; Heddergott, C.; Robinet, P.; Aimanianda, V.; Beau, R.; Beauvais, A.; Mouyna, I.; Prevost, M. C.; Fekkar, A.; Zhao, Y.; Perlin, D.; Latgé, J. P. Biosynthesis of Cell Wall Mannan in the Conidium and the Mycelium of Aspergillus Fumigatus. *Cell. Microbiol.* **2016**, *18* (12), 1881–1891. https://doi.org/10.1111/cmi.12665.

(63) Fontaine, T.; Latgé, J. P. Galactomannan Produced by Aspergillus Fumigatus: An Update on the Structure, Biosynthesis and Biological Functions of an Emblematic Fungal Biomarker. *J. Fungi* **2020**, *6* (4), 1–17. https://doi.org/10.3390/jof6040283.

(64) Engel, J.; Schmalhorst, P. S.; Routier, F. H. Biosynthesis of the Fungal Cell Wall Polysaccharide Galactomannan Requires Intraluminal GDP-Mannose. *J. Biol. Chem.* **2012**, *287* (53), 44418–44424. https://doi.org/10.1074/jbc.M112.398321.

(65) Toledano, V.; Hernández-Jiménez, E.; Cubillos-Zapata, C.; Flandez, M.; Álvarez, E.; Varela-Serrano, A.; Cantero, R.; Valles, G.; García-Rio, F.; López-Collazo, E. Galactomannan Downregulates the Inflammation Responses in Human Macrophages via NF κ B2/P100. *Mediators Inflamm.* **2015**, *2015*. https://doi.org/10.1155/2015/942517.

(66) Lass-Flörl, C. How to Make a Fast Diagnosis in Invasive Aspergillosis. *Med. Mycol.* **2019**, *57*, S155–S160. https://doi.org/10.1093/mmy/myy103.

(67) Henry, Christine, Jizhou Li, François Danion, Laura Alcazar-Fuoli, Emilia Mellado, Rémi Beau, Jean-Paul Latgé, T. F. Two KTR Mannosyltransferases Are Responsible for the Biosynthesis of Cell Wall Mannans and Control Polarized Growth in Aspergillus Fumigatus. *MBio* **2019**, *10* (1), 1–18. https://doi.org/doi.org/10.1128/mBio .02647-18.

(68) Fang, W.; Du, T.; Raimi, O. G.; Hurtado-Guerrero, R.; Mariño, K.; Ibrahim, A. F. M.; Albarbarawi, O.; Ferguson, M. A. J.; Jin, C.; Van Aalten, D. M. F. Genetic and Structural Validation of Aspergillus Fumigatus N-Acetylphosphoglucosamine Mutase as an Antifungal Target. *Biosci. Rep.* **2013**, *33* (5), 689–699. https://doi.org/10.1042/BSR20130053.

(69) Lockhart, D. E. A.; Stanley, M.; Raimi, O. G.; Robinson, D. A.; Boldovjakova, D.; Squair, D. R.; Ferenbach, A. T.; Fang, W.; van Aalten, D. M. F. Targeting a Critical Step in Fungal Hexosamine Biosynthesis. *J. Biol. Chem.* **2020**, *295* (19), jbc.RA120.012985. https://doi.org/10.1074/jbc.ra120.012985.

(70) Yan, K.; Stanley, M.; Kowalski, B.; Raimi, O. G.; Ferenbach, A. T.; Wei, P.; Fang, W.; van Aalten, D. M. F. Genetic Validation of Aspergillus Fumigatus Phosphoglucomutase as a Viable Therapeutic Target in Invasive Aspergillosis. *J. Biol. Chem.* **2022**, *298* (6), 102003. https://doi.org/10.1016/j.jbc.2022.102003.

(71) Sosicka, P.; Ng, B. G.; Freeze, H. H. Congenital Disorders of Glycosylation. *Compr. Glycosci. Second Ed.* **2021**, *6* (24), 294–334. https://doi.org/10.1016/B978-0-12-819475-1.00013-4.

(72) Mio, T.; Kokado, M.; Arisawa, M.; Yamada-Okabe, H. Reduced Virulence of Candida Albicans Mutants Lacking the GNA1 Gene Encoding Glucosamine-6-Phosphate Acetyltransferase. *Microbiology* **2000**, *146* (7), 1753–1758. https://doi.org/10.1099/00221287-146-7-1753.

(73) Fang, W.; Du, T.; Raimi, O. G.; Hurtado-Guerrero, R.; Urbaniak, M. D.; Ibrahim, A. F. M.; Ferguson, M. A. J.; Jin, C.; Van Aalten, D. M. F. Genetic and Structural Validation of Aspergillus FumigatusUDP-N-Acetylglucosamine Pyrophosphorylase as an Antifungal Target. *Mol. Microbiol.* **2013**, *89* (3), 479–493. https://doi.org/10.1111/mmi.12290.

(74) Hoffer, L.; Muller, C.; Roche, P.; Morelli, X. Chemistry-Driven Hit-to-Lead Optimization Guided by Structure-Based Approaches. *Mol. Inform.* **2018**, *37* (9). https://doi.org/10.1002/minf.201800059.

(75) Jhoti, H.; Williams, G.; Rees, D. C.; Murray, C. W. The “rule of Three” for Fragment-Based Drug Discovery: Where Are We Now? *Nat. Rev. Drug Discov.* **2013**, *12* (8), 644. https://doi.org/10.1038/nrd3926-c1.

(76) Köster, H.; Craan, T.; Brass, S.; Herhaus, C.; Zentgraf, M.; Neumann, L.; Heine, A.; Klebe, G. A Small Nonrule of 3 Compatible Fragment Library Provides High Hit Rate of Endothiapepsin Crystal Structures with Various Fragment Chemotypes. *J. Med. Chem.* **2011**, *54* (22), 7784–7796. https://doi.org/10.1021/jm200642w.

(77) Bentley, M. R.; Ilyichova, O. V.; Wang, G.; Williams, M. L.; Sharma, G.; Alwan, W. S.; Whitehouse, R. L.; Mohanty, B.; Scammells, P. J.; Heras, B.; Martin, J. L.; Totsika, M.; Capuano, B.; Doak, B. C.; Scanlon, M. J. Rapid Elaboration of Fragments into Leads by X-Ray Crystallographic Screening of Parallel Chemical Libraries (REFiLX). *J. Med. Chem.* **2020**, *63* (13), 6863–6875. https://doi.org/10.1021/acs.jmedchem.0c00111.

(78) Ichihara, O.; Barker, J.; Law, R. J.; Whittaker, M. Compound Design by Fragment-Linking. *Mol. Inform.* **2011**, *30* (4), 298–306. https://doi.org/10.1002/minf.201000174.

(79) Moerke, N. J. Fluorescence Polarization (FP) Assays for Monitoring Peptide-Protein or Nucleic Acid-Protein Binding. *Curr. Protoc. Chem. Biol.* **2009**, *1* (1), 1–15. https://doi.org/10.1002/9780470559277.ch090102.

(80) Catalano, M.; Moroglu, M.; Balbi, P.; Mazzieri, F.; Clayton, J.; Andrews, K. H.; Bigatti, M.; Scheuermann, J.; Conway, S. J.; Neri, D. Selective Fragments for the CREBBP Bromodomain Identified from an Encoded Self-Assembly Chemical Library. *ChemMedChem* **2020**, *15* (18), 1752–1756. https://doi.org/10.1002/cmdc.202000528.

(81) Li, Q. Application of Fragment-Based Drug Discovery to Versatile Targets. *Front. Mol. Biosci.* **2020**, *7* (August), 1–13. https://doi.org/10.3389/fmolb.2020.00180.

(82) Sultana, A.; Lee, J. E. Measuring Protein-Protein and Protein-Nucleic Acid Interactions by Biolayer Interferometry. *Curr. Protoc. Protein Sci.* **2015**, *2015*, 19.25.1-19.25.26. https://doi.org/10.1002/0471140864.ps1925s79.

(83) Wartchow, C. A.; Podlaski, F.; Li, S.; Rowan, K.; Zhang, X.; Mark, D.; Huang, K. Sen. Biosensor-Based Small Molecule Fragment Screening with Biolayer Interferometry. *J. Comput. Aided. Mol. Des.* **2011**, *25* (7), 669–676. https://doi.org/10.1007/s10822-011-9439-8.

(84) Ogura, Y.; Parsons, W. H.; Kamat, S. S.; Cravatt, B. F. Advantages of Crystallographic Fragment Screening: Functional and Mechanistic Insights from a Powerful Platform for Efficient Drug Discovery. *Physiol. Behav.* **2017**, *176* (10), 139–148. https://doi.org/10.1016/j.pbiomolbio.2014.08.004.Advantages.

(85) Zhou, Y.; Yan, K.; Qin, Q.; Raimi, O. G.; Du, C.; Wang, B.; Ahamefule, C. S.; Kowalski, B.; Jin, C.; van Aalten, D. M. F.; Fang, W. Phosphoglucose Isomerase Is Important for Aspergillus Fumigatus Cell Wall Biogenesis. *MBio* **2022**, *13* (4). https://doi.org/10.1128/mbio.01426-22.

(86) Beamer, L. J. Mutations in Hereditary Phosphoglucomutase 1 Deficiency Map to Key Regions of Enzyme Structure and Function. *J. Inherit. Metab. Dis.* **2015**, *38* (2), 243–256. https://doi.org/10.1007/s10545-014-9757-9.

(87) Stiers, K. M.; Graham, A. C.; Zhu, J. S.; Jakeman, D. L.; Nix, J. C.; Beamer, L. J. Structural and Dynamical Description of the Enzymatic Reaction of a Phosphohexomutase. *Struct. Dyn.* **2019**, *6* (2), 1–11. https://doi.org/10.1063/1.5092803.

(88) Raimi, O. G.; Hurtado-Guerrero, R.; Van Aalten, D. M. F. Evidence for Substrate-Assisted Catalysis in N-Acetylphosphoglucosamine Mutase. *Biochem. J.* **2018**, *475* (15), 2547–2557. https://doi.org/10.1042/BCJ20180172.

(89) Stiers, K. M.; Muenks, A. G.; Beamer, L. J. *Biology, Mechanism, and Structure of Enzymes in the α-D-Phosphohexomutase Superfamily*, 1st ed.; Elsevier Inc., 2017; Vol. 109. https://doi.org/10.1016/bs.apcsb.2017.04.005.

(90) Naught, L. E.; Regni, C.; Beamer, L. J.; Tipton, P. A. Roles of Active Site Residues in Pseudomonas Aeruginosa Phosphomannomutase/Phosphoglucomutase. *Biochemistry* **2003**, *42* (33), 9946–9951. https://doi.org/10.1021/bi034673g.

(91) Henry Christopher, J. van R.; Van den Ende, W. UDP-Glucose: A Potential Signaling Molecule in Plants? *Front. Plant Sci.* **2018**, *8* (January), 6–11. https://doi.org/10.3389/fpls.2017.02230.

(92) Beauvais, A.; Bozza, S.; Kniemeyer, O.; Formosa, C.; Balloy, V.; Henry, C.; Roberson, R. W.; Dague, E.; Chignard, M.; Brakhage, A. A.; Romani, L.; Latgé, J. P. Deletion of the α-(1,3)-Glucan Synthase Genes Induces a Restructuring of the Conidial Cell Wall Responsible for the Avirulence of Aspergillus Fumigatus. *PLoS Pathog.* **2013**, *9* (11). https://doi.org/10.1371/journal.ppat.1003716.

(93) Thammahong, A.; Puttikamonkul, S.; Perfect, J. R.; Brennan, R. G.; Cramer, R. A. Central Role of the Trehalose Biosynthesis Pathway in the Pathogenesis of Human Fungal Infections: Opportunities and Challenges for Therapeutic Development. *Microbiol. Mol. Biol. Rev.* **2017**, *81* (2). https://doi.org/10.1128/mmbr.00053-16.

(94) Regni, C.; Shackelford, G. S.; Beamer, L. J. Complexes of the Enzyme Phosphomannomutase/Phosphoglucomutase with a Slow Substrate and an Inhibitor. *Acta Crystallogr. Sect. F Struct. Biol. Cryst. Commun.* **2006**, *62* (8), 722–726. https://doi.org/10.1107/S1744309106025887.

(95) Yan, K. Targeting Final Steps of Sugar Nucleotide Biosynthetic Pathway against Aspergillus Fumigatus, University of Dundee, 2020.

(96) Baell, J. B.; Nissink, J. W. M. Seven Year Itch: Pan-Assay Interference Compounds (PAINS) in 2017 - Utility and Limitations. *ACS Chem. Biol.* **2018**, *13* (1), 36–44. https://doi.org/10.1021/acschembio.7b00903.

(97) Jasial, S.; Hu, Y.; Bajorath, J. How Frequently Are Pan-Assay Interference Compounds Active? Large-Scale Analysis of Screening Data Reveals Diverse Activity Profiles, Low Global Hit Frequency, and Many Consistently Inactive Compounds. *J. Med. Chem.* **2017**, *60* (9), 3879–3886. https://doi.org/10.1021/acs.jmedchem.7b00154.

(98) Baell, J. B.; Holloway, G. A. New Substructure Filters for Removal of Pan Assay Interference Compounds (PAINS) from Screening Libraries and for Their Exclusion in Bioassays. *J. Med. Chem.* **2010**, *53* (7), 2719–2740. https://doi.org/10.1021/jm901137j.

(99) Silva, V.; Silva, C.; Soares, P.; Garrido, E. M.; Borges, F.; Garrido, J. Isothiazolinone Biocides: Chemistry, Biological, and Toxicity Profiles. *Molecules* **2020**, *25* (4). https://doi.org/10.3390/molecules25040991.

(100) Estlander, T.; Jolanki, R.; Kanerva, L. Occupational Allergic Contact Dermatitis from 2,3-Epoxypropyl Trimethyl Ammonium Chloride (EPTMAC) and Kathon® LX in a Starch Modification Factory. *Contact Dermatitis* **1997**, *36* (4), 191–194. https://doi.org/10.1111/j.1600-0536.1997.tb00268.x.

(101) Stiers, K. M.; Kain, B. N.; Graham, A. C.; Beamer, L. J. Induced Structural Disorder as a Molecular Mechanism for Enzyme Dysfunction in Phosphoglucomutase 1 Deficiency. *J. Mol. Biol.* **2016**, *428* (8), 1493–1505. https://doi.org/10.1016/j.jmb.2016.02.032.

(102) Weitner, T.; Friganović, T.; Šakić, D. Inner Filter Effect Correction for Fluorescence Measurements in Microplates Using Variable Vertical Axis Focus. *Anal. Chem.* **2022**. https://doi.org/10.1021/acs.analchem.2c01031.

(103) Estupiñán, H. Y.; Wang, Q.; Berglöf, A.; Schaafsma, G. C. P.; Shi, Y.; Zhou, L.; Mohammad, D. K.; Yu, L.; Vihinen, M.; Zain, R.; Smith, C. I. E. BTK Gatekeeper Residue Variation Combined with Cysteine 481 Substitution Causes Super-Resistance to Irreversible Inhibitors Acalabrutinib, Ibrutinib and Zanubrutinib. *Leukemia* **2021**, *35* (5), 1317–1329. https://doi.org/10.1038/s41375-021-01123-6.

(104) Strelow, J. M. A Perspective on the Kinetics of Covalent and Irreversible Inhibition. *J. Biomol. Screen.* **2017**, *22* (1), 3–20. https://doi.org/10.1177/1087057116671509.

(105) Mons, E.; Roet, S.; Kim, R. Q.; Mulder, M. P. C. A Comprehensive Guide for Assessing Covalent Inhibition in Enzymatic Assays Illustrated with Kinetic Simulations. *Curr. Protoc.* **2022**, *2* (6), 1–85. https://doi.org/10.1002/cpz1.419.

(106) Pettinger, J.; Carter, M.; Jones, K.; Cheeseman, M. D. Kinetic Optimization of Lysine-Targeting Covalent Inhibitors of HSP72. *J. Med. Chem.* **2019**, *62* (24), 11383–11398. https://doi.org/10.1021/acs.jmedchem.9b01709.

(107) Shoichet, B. K. Interpreting Steep Dose-Response Curves in Early Inhibitor Discovery. *J. Med. Chem.* **2006**, *49* (25), 7274–7277. https://doi.org/10.1021/jm061103g.

(108) Morley, J. O.; Jayne, A.; Kapur, O.; Charlton, M. H. Structure – Activity Relationships in 3-Isothiazolones. **2005**, No. Scheme 2, 3713–3719.

(109) Swinney, D. Biochemical Mechanisms of New Molecular Entities (NMEs) Approved by United States FDA During 2001-2004: Mechanisms Leading to Optimal Efficacy and Safety. *Curr. Top. Med. Chem.* **2006**, *6* (5), 461–478. https://doi.org/10.2174/156802606776743093.

(110) Park, C. Visual Interpretation of the Meaning of Kcat/ KMin Enzyme Kinetics. *J. Chem. Educ.* **2022**, *99* (7), 2556–2562. https://doi.org/10.1021/acs.jchemed.1c01268.

(111) Boudart, M.; Djega-Mariadassou, G. Kinetics of Monosubstrate Reactions. In *Comprehensive Enzyme Kinetics*; Princeton University Press, (2015), 77-117, 2015; pp 77–117. https://doi.org/10.1515/9781400853335.77.

(112) Holdgate, G. A.; Meek, T. D.; Grimley, R. L. Mechanistic Enzymology in Drug Discovery: A Fresh Perspective. *Nat. Rev. Drug Discov.* **2018**, *17* (2), 115–132. https://doi.org/10.1038/nrd.2017.219.

(113) Niesen, F. H.; Schultz, L.; Jadhav, A.; Bhatia, C.; Guo, K.; Maloney, D. J.; Pilka, E. S.; Wang, M.; Oppermann, U.; Heightman, T. D.; Simeonov, A. High-Affinity Inhibitors of Human NAD+-Dependent 15-Hydroxyprostaglandin Dehydrogenase: Mechanisms of Inhibition and Structure-Activity Relationships. *PLoS One* **2010**, *5* (11). https://doi.org/10.1371/journal.pone.0013719.

(114) de Souza Neto, L. R.; Moreira-Filho, J. T.; Neves, B. J.; Maidana, R. L. B. R.; Guimarães, A. C. R.; Furnham, N.; Andrade, C. H.; Silva, F. P. In Silico Strategies to Support Fragment-to-Lead Optimization in Drug Discovery. *Front. Chem.* **2020**, *8* (February), 1–18. https://doi.org/10.3389/fchem.2020.00093.

(115) Luo, Q.; Tao, Y.; Sheng, W.; Lu, J.; Wang, H. Dinitroimidazoles as Bifunctional Bioconjugation Reagents for Protein Functionalization and Peptide Macrocyclization. *Nat. Commun.* **2019**, *10* (1), 1–9. https://doi.org/10.1038/s41467-018-08010-2.

(116) António, J. P. M.; Faustino, H.; Gois, P. M. P. A 2-Formylphenylboronic Acid (2FPBA)-Maleimide Crosslinker: A Versatile Platform for Cys-Peptide-Hydrazine Conjugation and Interplay. *Org. Biomol. Chem.* **2021**, *19* (28), 6221–6226. https://doi.org/10.1039/d1ob00917f.

(117) Belbekhouche, S.; Guerrouache, M.; Carbonnier, B. Thiol-Maleimide Michael Addition Click Reaction: A New Route to Surface Modification of Porous Polymeric Monolith. *Macromol. Chem. Phys.* **2016**, *217* (8), 997–1006. https://doi.org/10.1002/macp.201500427.

(118) Sippel, T. O. A Fluorescence-Based Assay for N-Myristoyltransferase Activity. *J. Histochem. Cytochem.* **1981**, *29* (2), 314–316. https://doi.org/10.1177/29.2.7019305.

(119) Li, X.; Zheng, Y.; Tong, H.; Qian, R.; Zhou, L.; Liu, G.; Tang, Y.; Li, H.; Lou, K.; Wang, W. Rational Design of an Ultrasensitive and Highly Selective Chemodosimeter by a Dual Quenching Mechanism for Cysteine Based on a Facile Michael-Transcyclization Cascade Reaction. *Chem. - A Eur. J.* **2016**, *22* (27), 9247–9256. https://doi.org/10.1002/chem.201601126.

(120) Goncalves, V.; Brannigan, J. A.; Thinon, E.; Olaleye, T. O. A Fluorescence-Based Assay for N-Myristoyltransferase Activity. **2013**, *421* (1), 1–7. https://doi.org/10.1016/j.ab.2011.10.013.A.

(121) Ercal, N.; Yang, P.; Aykin, N. Determination of Biological Thiols by High-Performance Liquid Chromatography Following Derivatization by ThioGlo Maleimide Reagents. *J. Chromatogr. B Biomed. Sci. Appl.* **2001**, *753* (2), 287–292. https://doi.org/10.1016/S0378-4347(00)00560-0.

(122) Hoff, S.; Larsen, F. H.; Andersen, M. L.; Lund, M. N. Quantification of Protein Thiols Using ThioGlo 1 Fluorescent Derivatives and HPLC Separation. *Analyst* **2013**, *138* (7), 2096–2103. https://doi.org/10.1039/c3an36672c.

(123) Klix, M. B.; Verreet, J. A.; Beyer, M. Comparison of the Declining Triazole Sensitivity of Gibberella Zeae and Increased Sensitivity Achieved by Advances in Triazole Fungicide Development. *Crop Prot.* **2007**, *26* (4), 683–690. https://doi.org/10.1016/j.cropro.2006.06.006.

(124) G. Wyatt, P.; H. Gilbert, I.; D. Read, K.; H. Fairlamb, A. Target Validation: Linking Target and Chemical Properties to Desired Product Profile. *Curr. Top. Med. Chem.* **2011**, *11* (10), 1275–1283. https://doi.org/10.2174/156802611795429185.

(125) Dahlin, J. L.; Walters, M. A. How to Triage PAINS-Full Research. *Assay Drug Dev. Technol.* **2016**, *14* (3), 168–174. https://doi.org/10.1089/adt.2015.674.

(126) Jumper, J.; Evans, R.; Pritzel, A.; Green, T.; Figurnov, M.; Ronneberger, O.; Tunyasuvunakool, K.; Bates, R.; Žídek, A.; Potapenko, A.; Bridgland, A.; Meyer, C.; Kohl, S. A. A.; Ballard, A. J.; Cowie, A.; Romera-Paredes, B.; Nikolov, S.; Jain, R.; Adler, J.; Back, T.; Petersen, S.; Reiman, D.; Clancy, E.; Zielinski, M.; Steinegger, M.; Pacholska, M.; Berghammer, T.; Bodenstein, S.; Silver, D.; Vinyals, O.; Senior, A. W.; Kavukcuoglu, K.; Kohli, P.; Hassabis, D. Highly Accurate Protein Structure Prediction with AlphaFold. *Nature* **2021**, *596* (7873), 583–589. https://doi.org/10.1038/s41586-021-03819-2.

(127) Keeley, A.; Petri, L.; Ábrányi-Balogh, P.; Keserű, G. M. Covalent Fragment Libraries in Drug Discovery. *Drug Discov. Today* **2020**, *25* (6), 983–996. https://doi.org/10.1016/j.drudis.2020.03.016.

(128) Szijj, P. A.; Bahou, C.; Chudasama, V. Minireview: Addressing the Retro-Michael Instability of Maleimide Bioconjugates. *Drug Discov. Today Technol.* **2018**, *30*, 27–34. https://doi.org/10.1016/j.ddtec.2018.07.002.

(129) Smith, M. E. B.; Schumacher, F. F.; Ryan, C. P.; Tedaldi, L. M.; Papaioannou, D.; Waksman, G.; Caddick, S.; Baker, J. R. Protein Modification, Bioconjugation, and Disulfide Bridging Using Bromomaleimides. *J. Am. Chem. Soc.* **2010**, *132* (6), 1960–1965. https://doi.org/10.1021/ja908610s.